Ecological Indicators 185 (2026) 114798

Contents lists available at ScienceDirect

Ecological Indicators

journal homepage: www.elsevier.com/locate/ecolind

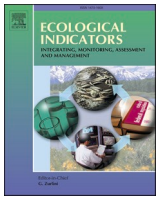

Multi-scale forest typologies using novel vertical layer metrics from airborne LiDAR in temperate mixed forests

Seunghyeon Lee [a,b], Uirin Ha [c], Heejae Lee [d], Hyeyeong Choe [c,e], Hansoo Kim [f], Youngkeun Song [a,b,g,*]

[a] Interdisciplinary Program in Landscape Architecture, Seoul National University, 1 Gwanak-ro, Gwanak-gu, Seoul 08826, Republic of Korea
[b] Integrated Major in Smart City Global Convergence, Seoul National University, 1 Gwanak-ro, Gwanak-gu, Seoul 08826, Republic of Korea
[c] Department of Agriculture, Forestry and Bioresources, College of Agriculture and Life Sciences, Seoul National University, 1 Gwanak-ro, Gwanak-gu, Seoul 08826, Republic of Korea
[d] National Forest Satellite Information & Technology Center, National Institute of Forest Science, 25 Godeokbizvalley-ro 1-gil, Gangdong-gu, Seoul 05203, Republic of Korea
[e] Research Institute of Agriculture and Life Sciences, Seoul National University, Seoul 08826, Republic of Korea
[f] Climate, Environment and Energy Research Division, Gyeonggi Research Institute, 1150 Gyeongsu-daero, Jangan-gu, Suwon 16207, Gyeonggi-do, Republic of Korea
[g] Department of Environmental Design, Graduate School of Environmental Studies, Seoul National University, 1 Gwanak-ro, Gwanak-gu, Seoul 08826, Republic of Korea

ARTICLE INFO

Keywords:
ALS
Forest structural classification
Vertical layer indices
PCA–HDBSCAN clustering
Scale dependence
Temperate mixed forest

ABSTRACT

Precisely quantifying forest vertical structure is fundamental to understanding biodiversity, productivity, and ecosystem functions. Airborne Laser Scanning (ALS) provides an unparalleled capacity to capture three-dimensional canopy architecture, yet existing metrics often overlook attributes of individual layers. To address these limitations, this study developed novel vertical layer indices, applied clustering, and tested robustness across scales. We used high-density ALS data (over 200 points·m^{-2}) covering 5.6 km^2 of temperate mixed forest in South Korea, encompassing diverse species compositions and successional stages. For scale-dependent analysis, circular analytical units with radii of 5- and 10-m were applied. A vertical layer segmentation procedure was optimized, achieving close agreement with field assessments (Mean Absolute Error ≈ 0.4 m), and provided the number of vertical layers and their ranges. From these results, ten indices were created to quantify layer height, gap size, and diversity at both species and unit scales. The indices were clustered into four to five interpretable types using Principal Component Analysis (PCA) and Hierarchical Density-Based Spatial Clustering of Applications with Noise (HDBSCAN), which explained over 70% of structural variance. For the 10-m units, the forest was classified as monolayer conifers, mixed mid-story, broadleaved multi-layer, stratified late-successional, and noise (structurally indeterminate units left unassigned), accounting for 31.8%, 39.8%, 11.3%, 5.9%, and 11.2%, respectively. Scale comparisons showed the Cumulative Layer Range (CLR) was stable, with differences within ±1.7% across six species out of eight. In contrast, Shannon's H′ was sensitive, increasing by 0.08 (25%) in 5-m units for *Pinus densiflora*. This index-based approach quantifies forest structural characteristics and captures scale-dependent vertical complexities.

1. Introduction

Forest structure, defined as the three-dimensional arrangement of vegetation, underpins core ecological functions, including biodiversity maintenance, microclimate regulation, and productivity (Oliver & Larson, 1996; Shugart et al., 2010). Because forest structure is continuously reshaped by competition, disturbance, and succession, its quantification is widely used as an indicator of forest condition and functionality (Ontl et al., 2020). Vertical stratification (the organization of vegetation into distinct layers from the forest floor to the upper

* Corresponding author at: Interdisciplinary Program in Landscape Architecture, Seoul National University, 1 Gwanak-ro, Gwanak-gu, Seoul 08826, Republic of Korea; Integrated Major in Smart City Global Convergence, Seoul National University, 1 Gwanak-ro, Gwanak-gu, Seoul 08826, Republic of Korea; Department of Environmental Design, Graduate School of Environmental Studies, Seoul National University, 1 Gwanak-ro, Gwanak-gu, Seoul 08826, Republic of Korea
E-mail addresses: shlee5598@snu.ac.kr (S. Lee), har2428@snu.ac.kr (U. Ha), heejae0110@korea.kr (H. Lee), hy.choe@snu.ac.kr (H. Choe), kimhs@gri.re.kr (H. Kim), songyoung@snu.ac.kr (Y. Song).

https://doi.org/10.1016/j.ecolind.2026.114798
Received 19 August 2025; Received in revised form 19 February 2026; Accepted 16 March 2026
Available online 24 March 2026

canopy) has been increasingly recognized as a central feature of ecosystem complexity and function (Ehbrecht et al., 2021). The arrangement of vegetation layers and the resulting vertical heterogeneity are closely linked to variation in species richness and abundance across taxa (MacArthur and MacArthur, 1961; Zellweger et al., 2013) and have also been associated with higher productivity and ecosystem stability through canopy packing and resource-use efficiency (Hardiman et al., 2011). Given these links to biodiversity, productivity, and ecosystem resilience, developing precise and scalable approaches to quantify vertical forest structure remains a key priority in forest ecology (Ehbrecht et al., 2017).

Traditionally, characterizing forest structure has relied on field investigations. While accurate at local scales, these methods are often labor-intensive, spatially restricted, and prone to subjectivity when describing continuous vertical arrangements (Zimble et al., 2003). Moreover, quantifying detailed vertical attributes from the ground—such as the precise height and thickness of individual layers or the size of vertical gaps between them—remains exceptionally challenging. Traditional field techniques struggle to consistently capture these subtle characteristics (Seidel et al., 2011). Although passive remote sensing such as satellite or airborne-acquired spectral imageries has facilitated landscape-scale assessments. Its two-dimensional nature restricts its capacity to capture the complicated details of vertical stratification. The advent of Light Detection and Ranging (LiDAR), particularly airborne laser scanning (ALS), has revolutionized forest structure analysis by providing direct, high-resolution three-dimensional measurements of canopy architecture (Lefsky et al., 2002; Wulder et al., 2008; Zhao et al., 2009). The ability of LiDAR to penetrate canopies and record returns from multiple vegetation layers, as well as the ground, makes it an unparalleled tool for quantifying vertical forest structure.

Leveraging this technology, numerous studies have developed methods to analyze vertical forest structure using LiDAR data. A primary focus has been on identifying the number and general position of canopy layers, ranging from analyzing vertical height histograms (Hamraz et al., 2017) and employing mixture distribution models (Jaskierniak et al., 2011) to applying machine learning techniques for strata classification (Wernicke et al., 2022). Other studies have aimed to summarize the entire vertical profile into a single complexity metric, such as height variance (Zimble et al., 2003), Foliage Height Diversity (FHD) (MacArthur and MacArthur, 1961; Hirschmugl et al., 2023), or canopy entropy (Liu et al., 2022). However, the effectiveness of these generalized methods is fundamentally challenged when applied to the structural intricacies of temperate mixed forests. These ecosystems are a mosaic of coexisting species with varied crown architectures and growth rates (Jucker et al., 2015), resulting in a highly complex and vertically heterogeneous canopy. Unlike structurally simpler forests, they often feature not just a dominant canopy and a ground layer, but also a congested sub-canopy of mid-story trees and a well-developed shrub layer (Deng et al., 2023), creating a continuous and overlapping vertical profile rather than discrete, easily separable strata (Atkins et al., 2018a, b). In such environments, methods currently utilized face inherent limitations for comprehensively understanding the vertical structure of temperate forests. Counting layers can overlook key features within- and between-layers, such as their thickness, vertical spacing, and relative contributions to overall canopy architecture. Conversely, while single complexity metrics like FHD provide a broad measure of heterogeneity, they often miss the specific structural configurations that underpin ecological function, such as differences in successional stage or habitat complexity. Therefore, there is a clear need—and a significant research gap—in developing a comprehensive suite of indices that can quantify multiple, diverse aspects of identified layers, enabling a more holistic understanding of vertical structure.

In this context, our primary research objective is to develop a LiDAR-based approach to classify vertical and horizontal structural types in a temperate mixed forest. We focus on vertical stratification, defined here as the separation of vegetation into distinguishable height layers, and additionally consider the vertical gaps between layers. Central to this framework is the development of ten new vertical layer indices derived from layer-segmentation results. Whereas conventional LiDAR metrics—such as height percentiles, FHD, or canopy volume measures—summarize overall vertical heterogeneity, they do not explicitly represent the geometry of individual layers, their thickness, or the vertical gaps that separate them. To address these limitations, our indices quantify complementary structural attributes: the lower and upper bounds of canopy layers (MIN, MAX), the total developed foliage space (CLR) and overall vertical span including voids (TR), the degree of interlayer porosity and compactness (AG, LDI), and the fine-scale variability and evenness of layer placement (RV, LRVI, HVI, H'). This multi-index framework allows a more detailed and ecologically interpretable representation of stratification than single-metric approaches and directly responds to the structural complexity characteristic of temperate mixed forests (Supplementary Table S1 summarizes index improvements over existing metrics).

Building on these indices, we apply Principal Component Analysis (PCA) together with Hierarchical Density-Based Spatial Clustering of Applications with Noise (HDBSCAN) to identify structural typologies without relying on predefined classes (Neuville et al., 2021; Moran et al., 2018; Gonçalves et al., 2024). Finally, we assess the sensitivity of these classifications to analytical unit scale (5-and 10-m radii) and examine how they vary across dominant tree species.

Finally, this study pursues three specific research objectives:

1. To develop ten vertical layer indices using ALS for quantifying and classifying forest vertical structure features and types in temperate mixed forests.
2. To cluster forest structural features using the ten vertical layer indices through PCA–HDBSCAN, enabling the identification of distinct structural typologies without relying on predefined classes.
3. To assess the effects of analytical unit scale (5- and 10-m) on vertical layer indices and clustering outcomes, and to interpret the ecological meaning of these scale sensitivities.

2. Study site and materials

The study was conducted in Yangju-si, Gyeonggi-do, Republic of Korea, covering an area of approximately 3.11 × 2.95 km (9.17 km^2) (Fig. 1a). This landscape represents a typical temperate mixed forest environment in the Korean Peninsula, encompassing a wide range of vertical and horizontal structure features. The terrain ranges from lowland valleys to hilly slopes, with elevations varying between 52 m and over 400 m above sea level (Fig. 1b), under a temperate climate with four distinct seasons.

Land-use and dominant species for forest were obtained from the official 2025 Urban Ecological Map of Gyeonggi Province produced by the Gyeonggi Research Institute. This dataset was generated through a full-scale field survey that covered all forest areas within Gyeonggi Province, including the present study site, providing spatially explicit land cover information, as well as the predominant and dominant species for each forest polygon. After excluding urbanized and military-restricted zones, the total forested area available for analysis was 5.65 km^2. While over 30 tree species are recorded, the main eight species—*Quercus mongolica, Pinus densiflora, Castanea crenata, Pinus rigida, Quercus aliena, Quercus acutissima, Pinus koraiensis, and Quercus variabilis*—account for more than 90% of the mapped polygons. Each of the remaining species contributes less than 1.5% of the total forested area. Therefore, analyses were focused on these eight dominant species.

The ALS survey was conducted on May 28, 2024, between 12:00 PM and 5:00 PM, at an average flight altitude of 1250 m and a flight speed of approximately 209 km/h. The resulting dataset achieved an high mean point-cloud density over 200 pts./m^2 in forested areas. Such resolution enables precise delineation of fine-scale vertical features, including

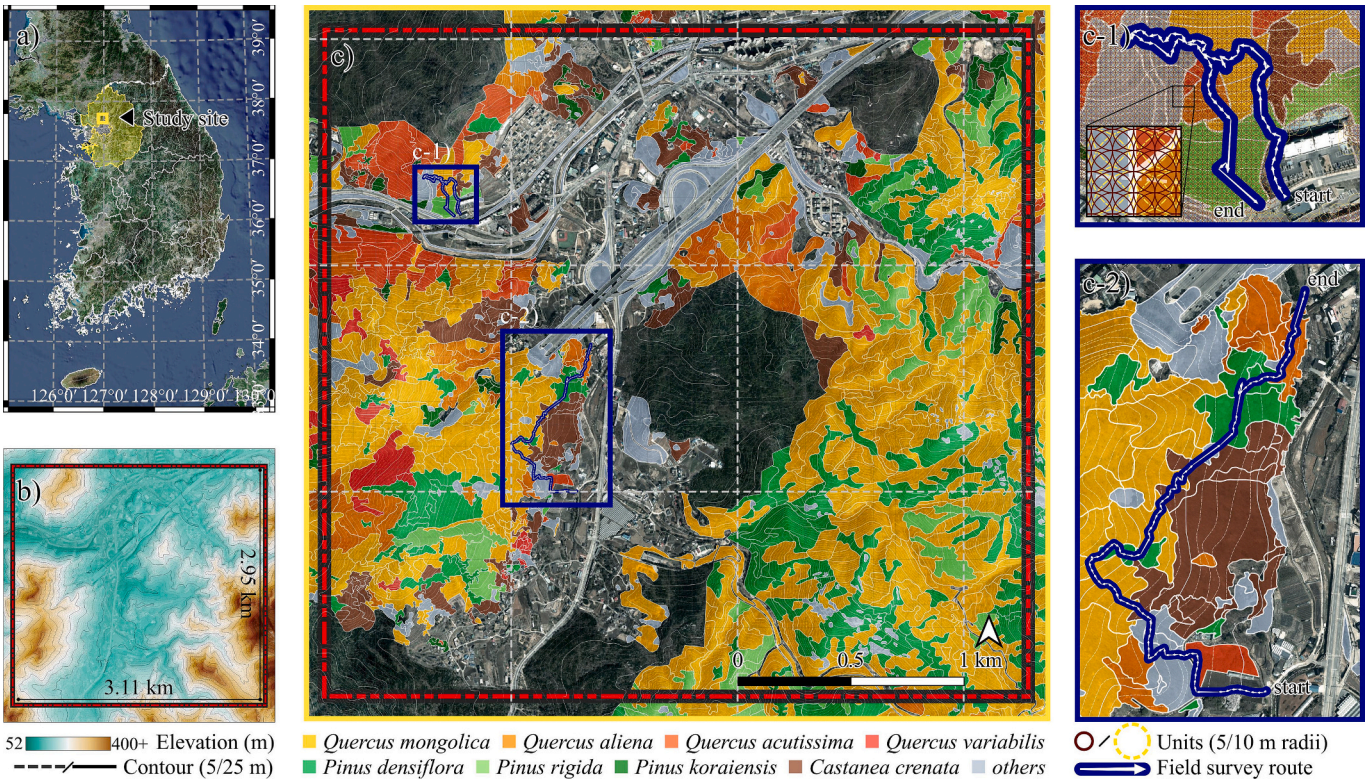

Fig. 1. Location of the study site and expert investigation routes. (a) Map of the Republic of Korea highlighting Gyeonggi-do and the study site; (b) Topographical map with 5 and 25 m contour lines; (c) Distribution of main eight tree species and others; (c-1) Northern investigation route. The enlarged black box shows the layout of 5- and 10-m radii circular analytical units; (c-2) Southern investigation route.

understorey vegetation, vertical gaps, and layer thickness. All analyses were performed at two spatial resolutions, using circular analytical units with radii of 5- and 10-m. This multi-scale design allowed us to examine how vertical layer indices and subsequent clustering outcomes respond to differences in analytical unit radii. Thereby, linking fine-scale and broader-scale structural variability across species and forest types.

3. Methods

3.1. Forest vertical layer segmentation using ALS dataset

To identify forest vertical layers, we applied a segmentation method to the pre-processed ALS dataset. The pre-processing involves point cloud outliers removal and classification into ground points, buildings, vegetation, roads, and power lines/towers. We then generated a CHM using the ground points and subsequently removed points associated with power infrastructure to minimize the error of vertical layer segmentation. The segmentation was conducted to circular analytic units that clipped by 5- and 10-m radii from ALS point cloud. The analytic units were clipped and used when they are fully contained by single forest inventory polygon. Through segmentation, we acquired the number of vertical layers and their height ranges.

Our segmentation process basically followed the protocol of Hamraz et al. (2017)'s method because its capacity to analyze the number and range of vertical layers and flexibility for parameter adjustment. This method is using circlular analytic units. For the points in the units, the canopy height histogram had drawn with the 0.25 m fixed binsize and smoothed the histogram line using the Gaussian kernel with standard deviation of 5-m. After smoothing, to pinpoint the layers, the second-derivative function applied to the smoothed line. And counted the number of ranges where the result was negative, as these indicate distinct vegetation layers.

3.2. Optimization of segmentation parameters and validation with field data

To ensure the accuracy of our layer detection, we first performed a systematic analysis to identify the optimal set of parameters for our study site. The accuracy of LiDAR-based analysis is highly sensitive to parameter choices, so we created 54 distinct calculation cases to test their impact (Table 1). This comprehensive evaluation was structured around three key factors.

First, to assess the effect of spatial scale, we tested two analytic unit radii for 5- and 10-m. These sizes align with standard forest inventory and allow for scale-dependency assessment. These sizes are consistent with multi-scale approaches where smaller units capture fine-scale understory details, while larger units effectively represent the dominant canopy structure (Frazer et al., 2011). The analytic units were generated to overlap with adjacent units by 5- and 10-m respectively (Fig. 1(c-1)).

Second, to account for ground returns and point cloud density, we evaluated three ground point filtering heights (1.0, 2.0, and 2.5 m) and three voxelization options (no voxelization, 0.25 m, and 0.5 m). Voxelization was tested as a key parameter to mitigate analytical biases caused by the uneven point densities inherent in ALS data (Vonderach et al., 2012). This process standardizes the point cloud into a regular 3D grid, yielding structural metrics that are more robust to sampling variations and better reflect the true vegetation architecture (Lecigne et al.,

Table 1
Unit radius and 3 kinds of parameter options.

Analytic unit radius (m)	voxelization (m)	ground point (m) filteringheight	histogram binsize (m) &Gaussiankernel
5	no voxelization	1.0	1.00 & 1.0
10	0.25	2.0	0.50 & 2.0
	0.5	2.5	0.25 & 4.0

2018).

Third, to find the best balance between histogram detail and smoothing, we tested three coupled settings of bin size and Gaussian kernel standard deviation. These were 0.25 m & 4.0 m, 0.5 m & 2.0 m, and 1.0 m & 1.0 m.

To identify the most accurate set of analytical parameters, we performed a optimization by validating 54 unique calculation cases (2 unit sizes × 27 parameter combinations) against expert field data. This validation data was collected by four experts of Korean forest and tree species for two separate investigations covering the northern and southern parts of the study site. Along two predefined field-survey routes (Fig. 1(c-1 & c-2)) where sampling points were established every 30 m and all analytical units intersected by the routes were inspected. During the investigations, paths were recorded using the Ramblr smartphone application. At each sampling location, observers stood at the plot center and assessed the canopy structure within a circular area matching the analytical-unit radius (5- or 10-m), determining the number of vertical layers formed by stratification through expert consensus. The determinations were recorded using the QField application. In total, 326 plots corresponding to 5-m units and 220 plots corresponding to 10-m units were surveyed.

Following the fieldwork, we calculated the Mean Absolute Error (MAE) and Mean Squared Error (MSE) between the expert investigation results and the 27 analytical results generated for each unit size. The entire analysis, applied to 120,404 units of 5-m radius and 17,961 of 10-m radius. As the 10-m analytical unit covers an area four times larger than a 5-m unit, the number of analytical units decreases at the coarser scale. Thus, the difference in sample size between 5- and 10-m units reflects the geometric relationship between scale and plot count, rather than an imbalance in sampling strategy or data availability. We analyzed the single analytical units with parallel processing acceleration through the Ray library in Python. For all further analyses, the results from the parameter set identified as the most accurate were used, ensuring our main findings are based on the most empirically validated method.

3.3. Definition of 10 vegetation vertical layer indices and comparison by speceis and unit sizes

To comprehensively capture the vertical structural features and heterogeneity of forest stands, we calculated ten quantitative indices based on the number of layers and the height ranges of each layer for every unit (Table 2, Fig. 2). Each index was designed to represent a specific aspect of forest vertical complexity and is classified into three classes that are layer height, layer gap, and layer diversity.

The layer height class includes the minimum and maximum layer heights (min and max), cumulative layer range (CLR), and total range (TR). The min and max indices respectively denote the lower and upper bounds of vegetation presence, corresponding to the initiation of the understory and the uppermost canopy elements. These two indices provide a fundamental profile of structural verticality and are particularly relevant for evaluating forest maturity. The CLR extends this perspective by summing the height ranges of all identified layers within a analytical unit, thereby offering a measure of total vertical foliage development. In contrast, the TR considers only the difference between the lowest and highest layer heights, emphasizing the absolute vertical extent rather than internal complexity.

The layer gap class includes two indices that of average gap (AG) and the Layer Density Index (LDI), which are represent the vertical discontinuity. The AG was calculated using the gaps between successive layers. This metric reflects the vertical openness or compactness of the vertical structure and is sensitive to structural fragmentation, often associated with disturbances or early successional stages. Building on this, the LDI relates the number of layers to the AG, providing a normalized measure of layer density. Higher LDI values indicate closely packed vegetation layers and a more vertically compact structure, which may enhance habitat availability and microclimate regulation.

Table 2
Ten vertical layer indices with definitions and equations.

Index	Class	Definition	Equation
MIN	layer height	Start height of lowermost layer height range	$(start_i)$
MAX	layer height	End height of uppermost layer height range	(end_n)
CLR (Cumulative Layer Range)	layer height	Sum of layer height ranges of all layers	$\sum_{i=1}^{n} (end_i - start_i)$
TR (Total Range)	layer height	Height range from the start to end of the first and last layers	$MAX - MIN$
AG (Average Gap)	layer gap	Average height gap between all layers	$\frac{\sum_{i=1}^{n-1} (start_{i+1} - end_i)}{n-1}$ $(if\ n > 1, otherwise\ 0)$
LDI (Layer Density Index)	layer gap	Divide the number of layers by average gap	$\frac{n}{AG+1}$
RV (Range Variance)	layer diversity	Variance of the height ranges of all layers	$\left(\frac{1}{n}\right)\sum_{i=1}^{n} ((end_i - start_i) - \bar{r})^2$ $(where\ \bar{r}\ is\ the\ mean\ height\ range)$
LRVI (Layer Range Variability Index)	layer diversity	Divide the range variance by the number of layers	$\frac{RV}{n+1}$
HVI (Height Variability Index)	layer diversity	Divide the standard deviation of layer heights by the mean layer height	$\frac{\sigma H}{MLH}$
VLD (Vertical Layer Diversity)	layer diversity	Layer height diversity based on the height range proportion of all layers. Based on the Shannon diversity index.	$-\sum_{i=1}^{n} p_i ln(p_i)$ $where\ p_i = \frac{(end_i - start_i)}{\sum_{i=1}^{n} (end_i - start_i)}$

Finally, the layer diversity class comprises four indices. The Range Variance (RV) quantifies the variability in thickness across individual layers, capturing differences in foliage accumulation and vertical growth forms. The Layer Range Variability Index (LRVI) further refines RV by accounting for the number of layers, enabling comparisons across analytical units with varying vertical structural intensity while isolating internal variability. To evaluate the relative dispersion of vertical positions, the Height Variability Index (HVI) was defined by dividing the standard deviation by the mean height of each layer. This dimensionless metric captures the irregularity in vertical layer placement, which is a key attribute of structural complexity. Lastly, we analyzed the Shannon's diversity based Vertical Layer Diversity (VLD), adapted to reflect the proportional distribution of vertical space occupied by each layer. This index integrates both the number of layers and the evenness of their height contributions, thus serving as a robust indicator of vertical stratification complexity. Together, these indicators provide a multidimensional framework for assessing forest vertical structure, allowing for detailed characterization and comparative analysis of vegetation

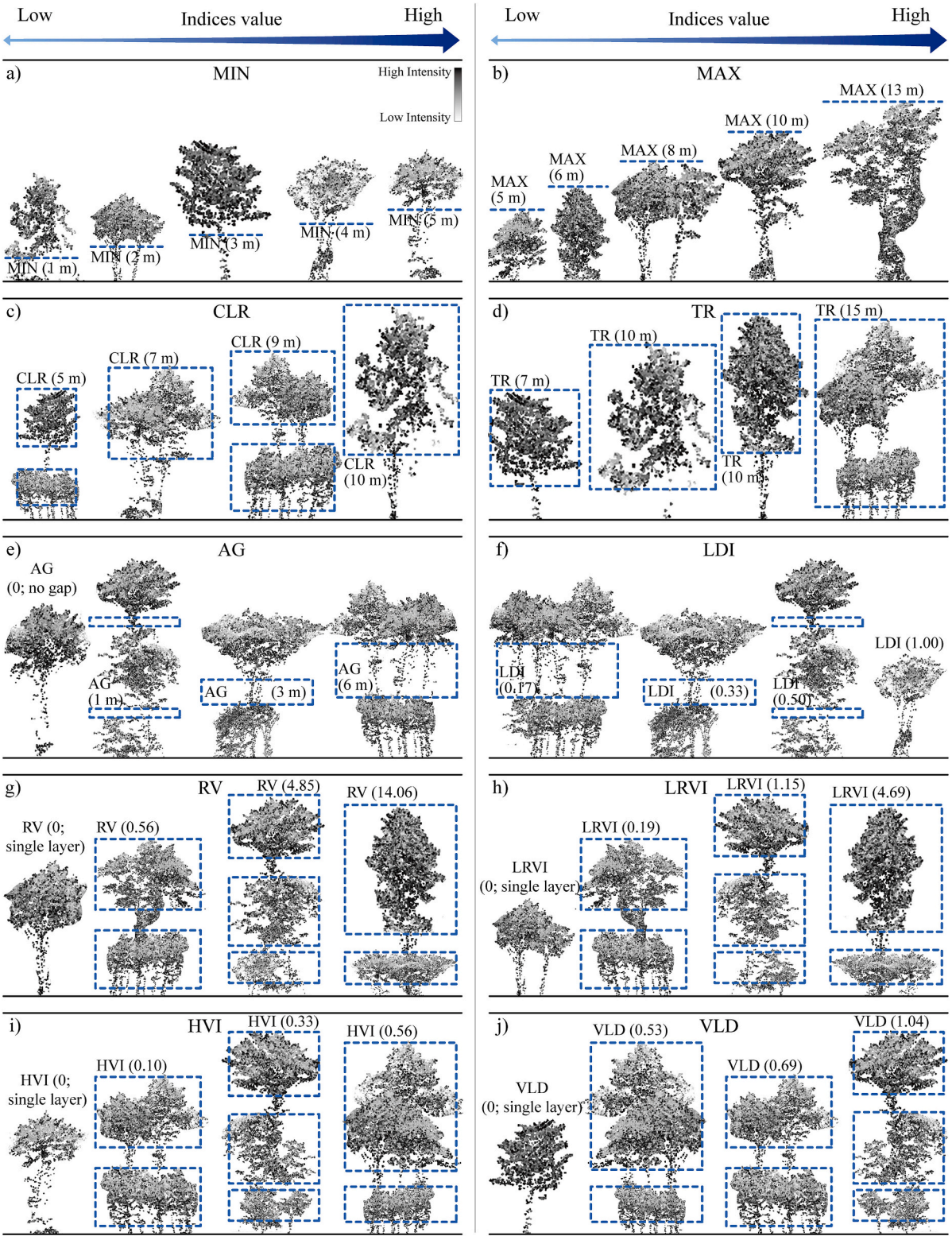

Fig. 2. ALS point cloud based canopy cross-sections showing ten vertical layer indices variation, arranged from low to high values. (a) MIN; (b) MAX; (c) CLR; (d) TR; (e) AG; (f) LDI; (g) RV; (h) LRVI; (i) HVI; (j) VLD.

development and stratification patterns.

For the entire 5- and 10-m radii units, ten vertical layer indices were calculated. By the eight kinds of main species, the average and variance of those ten indices were computed. And the *t*-test was conducted between the 5- and 10-m radii analytical units indices to calculate the *p*-value. The differences and the ratio of these differences to the 5-m analytical unit results were also derived to quantify the magnitude of change. These statistics were employed to characterize the vertical structural aspects by species and to quantify the structural feature differences derived from analytical unit size.

3.4. Dimensionality reduction and clustering of vegetation structural indices

To classify distinct patterns of vegetation vertical structure across the study site, we performed unsupervised clustering based on a dimensionality-reduced feature space. The ten vertical layer indices that quantitatively represent the canopy heights, gap distribution, and vertical heterogeneity (Table 2) were used. This procedure was conducted independently for two datasets based on 5- and 10-m radii analytical units. To reduce data dimensionality while retaining most of the information in the ten vertical layer indices prior to clustering, we used PCA. A similar PCA-based step has been used in LiDAR forest-structure studies to summarize multi-metric structural information (Montoya-Sánchez et al., 2024). PCA was applied to the standardized values of the ten indices and transforms the original correlated variables into a new set of uncorrelated variables called Principal Components (PCs). Each PC captures successively smaller portion of the total variance, representing structural variability across analytical units. The first two PCs (PC1 and PC2) were retained for visualization and clustering in both the 5- and 10-m radii analytical unit datasets. Here, PCs are used only to obtain the feature space for clustering. The resulting forest types are interpreted by profiling each cluster using the original ten vertical layer indices, summarized as cluster-wise mean values (and corresponding variability), with PC loadings used only as a supplementary guide.

Following dimensionality reduction, we employed the Hierarchical Density-Based Spatial Clustering of Applications with Noise (HDBSCAN) algorithm (McInnes et al., 2017) to identify structurally distinct analytical unit groups in the PCA space. This PCA–HDBSCAN approach has proven its effectiveness for grouping structurally or functionally similar units (e.g., forest patches, plots, or strata) based on LiDAR-derived metrics (e.g., Féret and Asner, 2012). Unlike k-means or Gaussian mixture models, HDBSCAN does not require a predefined number of clusters. It is robust to noise and clusters of varying densities, making it particularly well-suited for ecological data that may contain outliers or exhibit gradual transitions.

The PCA–HDBSCAN clustering was performed using only the ten vertical layer indices, independent of species information or abundance. Thus, differences in sample size among species reflect the natural composition of the study area and do not influence cluster formation. After clustering, to interpret the resulting structural typologies in ecological terms, we subsequently examined the relative proportions of the eight dominant tree species within each cluster. Rather than assigning a single species to each cluster, this post hoc analysis provided a descriptive link indicating which species tended to dominate or co-occur in particular structural types. Each resulting cluster was visualized in PCA space. Clusters were relabeled alphabetically based on their mean PC1 orders, while noise points were retained and labeled separately. Additionally, we overlaid PCA loading vectors to interpret the influence of each index on the resulting component axes.

4. Results

4.1. Validation of layer segmentation results

Our ALS-based layer segmentation method demonstrated a high level of agreement with the expert field investigation. Overall, the best-performing parameter sets achieved a MAE of approximately 0.4, meaning our analysis typically deviated from the ground truth by less than half a layer. The results of all 27 parameter combinations tested in the optimization experiment are summarized in Supplementary Table S2, which is organized by voxelization, ground-filtering height, and histogram–kernel settings. In addition, for the ten most accurate parameter combinations, MAE and MSE for both 5- and 10-m analytical-unit radii are displayed as a back-to-back bar chart (Fig. 3).

A detailed analysis of the parameters revealed that their influence on accuracy varied, with some settings proving more critical than others. The ground point filtering height and the histogram settings emerged as the most consistently influential factors. For both 5- and 10-m analytical units, a filtering height of 1.0 m paired with a histogram set of a 1.0 m bin size and a 1.0 m Gaussian kernel reliably produced the most robust and accurate results among all tested combinations. In contrast, the effect of voxelization was less critical, though it did show a slight scale-

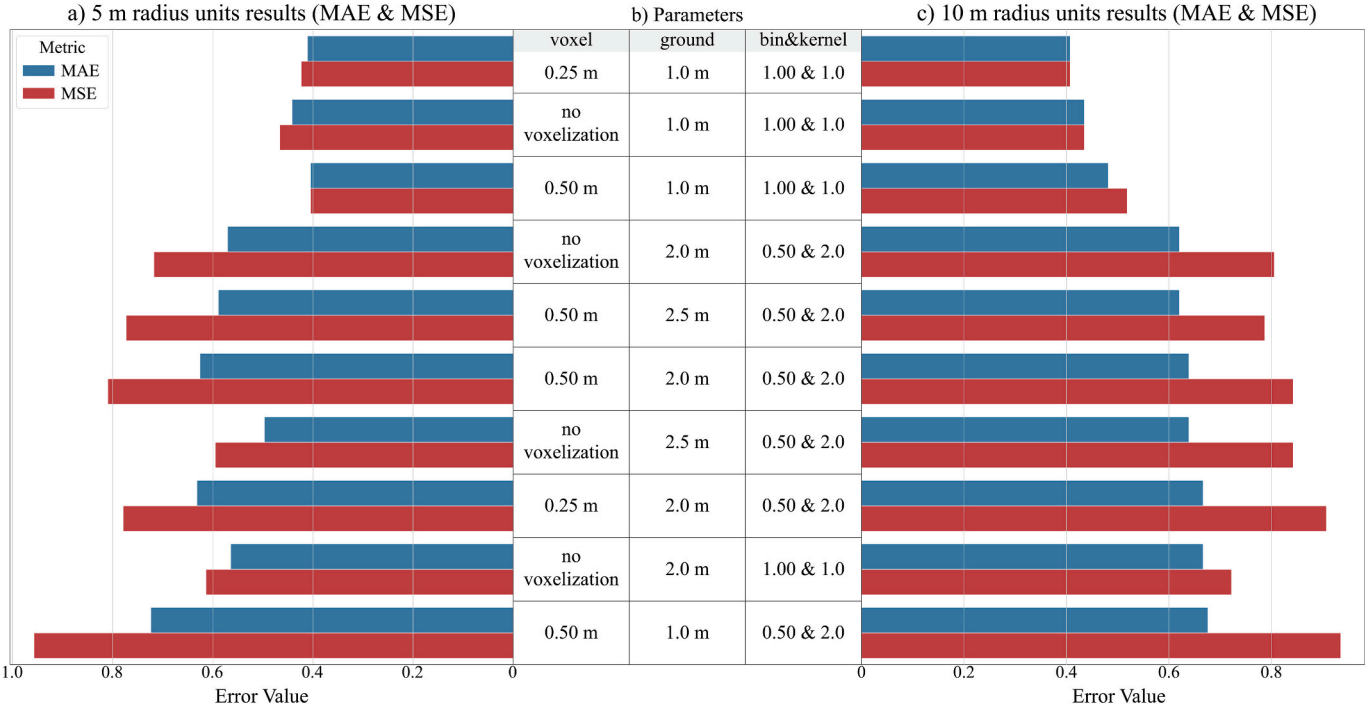

Fig. 3. Error comparison of ALS-based vertical layer segmentation parameter combinations. (a) Mean Absolute Error (MAE) and Mean Squared Error (MSE) for the ten best-performing parameter sets in 5-m radius analytical units. (b) Summary of the corresponding parameter combinations (voxelization, ground point filtering height, and histogram bin size–Gaussian kernel). (c) MAE and MSE for the same parameter sets in 10-m radius analytical units.

dependency. For the smaller 5-m units, a 0.5 m voxelization yielded the lowest error (MAE = 0.405), but the difference compared to the 0.25 m option was negligible. For the larger 10-m units, the 0.25 m voxelization was optimal, producing the lowest MAE and MSE (both 0.407).

Based on these validation results, we selected a single, optimal parameter set for all subsequent analyses to ensure consistency across both unit sizes: 0.25 m voxelization, 1.0 m ground point filtering height, and a 1.0 m bin size with a 1.0 m Gaussian kernel. The final layer segmentation maps derived using this optimized method are presented for both the 5- and 10-m analytical units (Fig. S1a and Fig. S2a, respectively).

4.2. Statistical analysis of 10 vertical layer indices by species and unit sizes

Forest vertical layer indices exhibit distinct species dependence and vary in sensitivity to analytical unit sizes (Table 3). Broadleaved deciduous species, such as *C. crenata*, *Q. acutissima*, and *Q. variabilis*, consistently showed greater structural complexity than conifers. While coniferous species maintained vertically compact and homogeneous structures across both analytical-unit sizes.

To characterize basic vertical extent and canopy development, we first examined the layer height indices MIN, MAX, CLR, and TR (Figs. S1b–e, S2b–e). The MAX index highlighted species-specific dominance in the upper strata: in 5-m units, the tallest canopies were found in *Q. acutissima* (19.31 m), *C. crenata* (18.85 m), and *P. koraiensis* (18.89 m), whereas *P. densiflora* had the lowest MAX (13.51 m) (Table 3a). These MAX values significantly decreased in 10-m units, reflecting the smoothing effect of the coarser footprint (Table 3c). The MIN showed the most significant relative decrease in *Q. variabilis* (−22.26%), a change that was statistically significant ($p < 0.05$), highlighting the influence of scale on identifying lower canopy initiation points.

CLR and TR, which quantify developed foliage space and total vertical span, showed similar species ranking across scales. Consistent with their definitions, TR values were approximately 50% larger than CLR across all species. Most CLR values remained stable between scales (ΔCLR within ±0.12 m for six species), underscoring the robustness of this metric, while TR exhibited greater variability due to the inclusion of gap space.AG and LDI characterize vertical porosity and compactness (Fig. S1f–g; Fig. S2f–g). In 5-m units, AG was widest in broadleaved species such as Q. aliena (4.74 m) and *Q. variabilis* (4.51 m), indicating well-separated layers (Table 3a). In contrast, *P. densiflora* exhibited extremely small AG values, reflecting its compact, single-layered canopy. Most broadleaved species exhibited statistically significant declines in AG at 10-m scale, reflecting the integration of micro-gaps within larger units.

The LDI index, which measures compactness, was highest in *P. densiflora* highlighting their dense layering. Broadleaved species such as Q. aliena (0.51) showed the lowest compactness, consistent with more open vertical structures. While absolute LDI differences were small by scales, several species showed notable proportional changes, such as *C. crenata* (+11.56%) and *Q. acutissima* (+9.33%), indicating differential sensitivity to vertical spacing and layer density across scales.Finally, we evaluated structural heterogeneity using layer diversity indices that of RV, LRVI, HVI, and H′ (Figs. S1h–k, S2h–k). Broadleaved species consistently exhibited higher structural irregularity than conifers. In 5-m units, RV was highest in *Q. variabilis* (1.31), *Q. acutissima* (1.27), and *C. crenata* (1.26), whereas *P. densiflora* showed the lowest value (0.68) (Table 3a). LRVI displayed a similar pattern, with *Q. variabilis* (0.40) representing the most variable layer structure and *P. densiflora* (0.21) the most uniform. Both RV and LRVI decreased at 10-m scale for most species, reflecting the loss of fine-scale heterogeneity as local structures are merged within larger footprints.

The HVI index highlighted species-specific differences in layer dispersion: in 5-m units, Q. aliena (0.46), *C. crenata* (0.45), and *P. koraiensis* (0.45) exhibited highly stratified canopies, whereas *P. densiflora* remained vertically uniform (0.22). HVI changed only marginally with scale, indicating relatively stable vertical positioning of layers. H′, the Shannon-based layer diversity metric, revealed the strongest gradient in overall structural complexity, ranging from *C. crenata* and *P. koraiensis* (0.74) to *P. densiflora* (0.31). H′ also showed the greatest sensitivity to scale: values increased by 25% for *P. densiflora* and 20.84% for *Q. variabilis* (Table 3d).

4.3. Canopy typologies and scale effects from PCA–HDBSCAN clustering

The PCA–HDBSCAN analysis revealed four to five distinct structural clusters (labeled A to E) and one noise group, each representing characteristic combinations of canopy layering, vertical distribution, and diversity (Figs. 4 and 5). These clusters consistently emerged in both the 5- and 10-m raddi analytical unit datasets, reinforcing the robustness of structure-based classification (Figure. Sl and Fig. S2). Clusters were defined based on ten vertical layer indices, which included height-based (min, max, CLR, TR), gap-based (AG, LDI), and diversity-based indices (RV, LRVI, HVI, VLD). In the 5-m radius unit dataset, the first two principal components explained 59.4% (PC1) and 14.5% (PC2) of the variance, respectively. For the 10-m dataset, PC1 and PC2 explained 62.7% and 13.5% of the total variance, respectively. These results demonstrate a strong capacity for dimensional reduction, with PC1 capturing the majority of variability (Figs. 4a and 5a). Cluster-wise species proportions differed across structural clusters. For example, conifers tended to occur at higher relative proportions in simple monolayer types (Cluster A), whereas broadleaved species were more frequently represented in multilayer or stratified clusters. These petterns were used to contextualize each structural cluster ecologically, rather than to define clusters by species identity.

Cluster A of both unit sizes consistently captured the simplest vertical structural type, defined by the absence of layering complexity and diversity. With nearly zero values in AG, RV, LRVI, HVI, and VLD (all 0.000 in 5-m and approximately 0.000 10-m), and a perfect LDI score of 1.000 for both unit sizes (Table 4). Cluster A exemplifies monolayered, vertically compact, and highly homogeneous forest stands. This structural uniformity is indicative of early-successional stages or dominated by even-aged coniferous species such as *P. densiflora* and *P. rigida* (5-m A: 14,219 units, 10-m A: 2264 units) (Table 5). In terms of proportion, Cluster A accounted for 26.0% of all 5-m units and 31.8% of all 10-m units, and its consistent appearance across different scales highlights the robustness of canopy structure simplification (Figs. 4(b1) and 5(b1)). Cluster A also showed relatively low average MAX and CLR values compared to other clusters (5-m: MAX = 12.466, CLR = 4.269; 10-m: MAX = 14.604, CLR = 4.662). This suggests that these stands are structurally simple, not only in terms of stratification but also in their overall vertical extent.

Clusters B and C in the 5-m dataset occupied an intermediate structural gradient and collectively corresponded to Cluster B in the 10-m radius units. Both 5-m clusters exhibited moderate structural metrics (RV: 0.467–1.237; LRVI: 0.127–0.358; VLD: 0.762–0.844), which were averaged and integrated into the broader 10-m radius unit Cluster B (RV: 0.979; LRVI: 0.290; VLD: 0.759) (Table 4). These clusters represented forests with layered yet somewhat regular structures, indicative of moderately stratified canopies with partial vertical development. Notably, the species compositions showed substantial representation from both broadleaf and coniferous species, implying structural hybridization. Cluster B accounted for 28.3% (B) and 22.0% (C) of 5-m units, and 39.8% of 10-m units, with the consolidation of Clusters B and C at the larger scale indicating that increasing the sampling area smooths localized variations and captures overarching structural trends (Figs. 4(b2–b3) and 5(b2)). These clusters exhibited significant heterogeneity in species composition compared to other clusters. Especially, in the 10-m radius units, *Q. mongolica* was relatively less abundant (48.95%) than in other clusters, while *C. crenata* (10.31%), *Q. aliena*

Table 3
Statistical summary of ten vertical layer indices for eight dominant species by unit scale. (a) Mean and variance (5-m units); (b) Mean and variance (10-m units); (c) Absolute mean differences (5 m – 10 m) with *t*-test *p*-values (*$p < 0.05$, **$p < 0.01$, ***$p < 0.001$); (d) Relative differences as percentage change from 5-m results.

Species	*Quercus mongolica*		*Pinus densiflora*		*Castanea crenata*		*Quercus aliena*		*Pinus rigida*		*Quercus acutissima*		*Quercus variabilis*		*Pinus koraiensis*	
(a)	5-m radius analytical units															
Number of units	61,756		21,569		8,818		8,662		8,529		6,869		2,465		1,736	
Statistics	Mean	Var	Mean	Var	Mean	Var	Mean	Var	Mean	Var	Mean	Var	Mean	Var	Mean	Var
MIN	4.28	6.74	4.15	5.44	4.35	7.78	4.20	6.85	4.03	5.96	4.57	7.90	4.63	11.35	4.25	5.16
MAX	16.83	12.46	13.51	15.55	18.85	7.25	18.82	6.59	16.08	13.19	19.31	9.95	18.28	5.90	18.89	8.87
CLR	6.61	3.90	5.29	3.32	7.46	3.69	7.42	3.52	6.36	3.94	7.43	4.32	6.82	3.16	7.68	3.60
TR	11.08	21.62	7.61	19.71	13.40	15.38	13.68	15.77	10.34	21.09	13.55	19.84	12.49	18.11	13.64	14.61
AG	3.47	7.29	1.97	6.67	4.40	5.90	4.74	6.52	3.43	7.68	4.50	6.46	4.51	7.72	4.47	5.24
LDI	0.63	0.09	0.77	0.09	0.55	0.08	0.51	0.07	0.60	0.09	0.54	0.08	0.52	0.08	0.52	0.07
RV	1.16	1.69	0.68	1.23	1.26	1.62	1.25	1.51	1.01	1.51	1.27	1.65	1.31	1.57	1.26	1.51
LRVI	0.35	0.16	0.21	0.12	0.36	0.14	0.36	0.13	0.32	0.15	0.36	0.14	0.40	0.15	0.36	0.13
HVI	0.37	0.06	0.22	0.07	0.45	0.03	0.46	0.03	0.36	0.06	0.44	0.04	0.44	0.05	0.45	0.03
VLD	0.58	0.13	0.31	0.14	0.74	0.09	0.73	0.08	0.50	0.12	0.72	0.10	0.64	0.10	0.74	0.08
(b)	10-m radius analytical units															
Number of units	9,251		2,913		1,469		1,259		1,255		1,203		427		184	
Statistics	Mean	Var	Mean	Var	Mean	Var	Mean	Var	Mean	Var	Mean	Var	mean	Var	Mean	Var
MIN	4.61	8.87	4.39	6.30	4.58	10.56	4.53	10.34	4.11	6.78	4.80	9.71	5.66	20.35	4.50	5.89
MAX	15.48	13.60	11.66	15.86	17.95	5.00	18.02	5.88	14.47	14.82	18.42	8.89	17.43	4.73	18.11	9.05
CLR	6.53	3.44	5.23	2.66	7.36	3.60	7.17	3.51	6.43	3.95	7.31	4.18	6.36	3.06	7.66	3.67
TR	10.87	22.29	7.28	18.29	13.37	15.21	13.49	18.59	10.36	22.02	13.61	21.07	11.77	24.19	13.61	13.44
AG	3.66	10.11	1.84	7.89	5.01	8.28	5.29	9.58	3.62	9.60	5.02	8.53	4.71	12.41	4.99	6.34
LDI	0.61	0.11	0.79	0.09	0.48	0.08	0.47	0.08	0.58	0.10	0.49	0.08	0.52	0.10	0.46	0.06
RV	1.27	2.12	0.67	1.44	1.39	1.87	1.23	1.62	1.01	1.59	1.42	1.94	1.35	1.83	1.29	1.55
LRVI	0.39	0.20	0.22	0.15	0.42	0.17	0.37	0.15	0.32	0.16	0.42	0.16	0.43	0.19	0.39	0.14
HVI	0.36	0.07	0.19	0.07	0.45	0.04	0.46	0.05	0.35	0.07	0.44	0.05	0.41	0.07	0.45	0.03
VLD	0.48	0.13	0.23	0.11	0.65	0.08	0.63	0.09	0.45	0.11	0.64	0.10	0.51	0.11	0.67	0.07
(c)	delta (5 m - 10 m) and p-value															
Statistics	Mean	Var	Mean	Var	Mean	Var	Mean	Var	Mean	Var	Mean	Var	Mean	Var	Mean	Var
MIN	−0.33	−2.13	−0.24	−0.86	−0.23	−2.78	−0.33	−3.49	−0.08	−0.82	−0.23	−1.81	−1.03	−9.00	−0.25	−0.73
	0.000***		0.000***		0.018*		0.000***		0.31		0.014*		0.048*		0.003**	
MAX	1.36	−1.13	1.85	−0.31	0.90	2.25	0.80	0.70	1.61	−1.62	0.89	1.06	0.85	1.18	0.78	−0.18
	0.000***		0.000***		0.000***		0.000***		0.000***		0.000***		0.000***		0.000***	
CLR	0.08	0.45	0.06	0.66	0.10	0.08	0.26	0.01	−0.07	−0.01	0.12	0.14	0.46	0.10	0.01	−0.07
	0.000***		0.07		0.08		0.000***		0.27		0.06		0.88		0.001***	
TR	0.22	−0.67	0.34	1.42	0.03	0.18	0.19	−2.82	−0.02	−0.93	−0.06	−1.23	0.72	−6.08	0.03	1.17
	0.000***		0.000***		0.78		0.12		0.87		0.66		0.88		0.06	
AG	−0.19	−2.82	0.12	−1.22	−0.61	−2.37	−0.55	−3.05	−0.19	−1.92	−0.52	−2.07	−0.20	−4.69	−0.51	−1.09
	0.000***		0.024*		0.000***		0.000***		0.036*		0.000***		0.000***		0.46	
LDI	0.01	−0.02	−0.02	0.00	0.06	0.00	0.05	−0.01	0.02	−0.01	0.05	0.00	0.01	−0.02	0.07	0.01
	0.000***		0.002**		0.000***		0.000***		0.045*		0.000***		0.000***		0.70	
RV	−0.11	−0.44	0.00	−0.20	−0.13	−0.26	0.02	−0.11	0.01	−0.08	−0.16	−0.30	−0.04	−0.27	−0.03	−0.05
	0.000***		0.96		0.002**		0.65		0.84		0.000***		0.64		0.68	
LRVI	−0.04	−0.05	0.00	−0.03	−0.06	−0.03	−0.01	−0.02	−0.01	−0.02	−0.06	−0.03	−0.03	−0.04	−0.02	−0.01
	0.000***		0.56		0.000***		0.34		0.62		0.000***		0.22		0.39	
HVI	0.02	−0.01	0.03	0.00	−0.01	−0.01	0.00	−0.01	0.01	−0.01	−0.01	−0.01	0.03	−0.02	0.00	0.00
	0.000***		0.000***		0.14		0.94		0.39		0.37		0.91		0.21	
VLD	0.09	0.01	0.08	0.03	0.09	0.00	0.09	0.00	0.05	0.01	0.07	0.00	0.13	−0.01	0.07	0.01
	0.000***		0.000***		0.000***		0.000***		0.000***		0.000***		0.000***		0.000***	
(d)	The ratio of delta to the 5-m radius analytical unit results (unit: %)															

(*continued on next page*)

Table 3 (*continued*)

Species	*Quercus mongolica*		*Pinus densiflora*		*Castanea crenata*		*Quercus aliena*		*Pinus rigida*		*Quercus acutissima*		*Quercus variabilis*		*Pinus koraiensis*	
Statistics	Mean	Var	Mean	Var	Mean	Var	Mean	Var	Mean	Var	Mean	Var	Mean	Var	Mean	Var
MIN	−7.78	−31.55	−5.69	−15.76	−5.27	−35.74	−7.81	−50.90	−1.96	−13.78	−5.15	−22.94	−22.26	−79.32	−5.86	−14.07
MAX	8.06	−9.09	13.67	−2.01	4.80	31.07	4.25	10.66	9.99	−12.29	4.60	10.68	4.65	19.91	4.13	−1.98
CLR	1.24	11.63	1.12	19.88	1.35	2.28	3.46	0.17	−1.04	−0.28	1.64	3.22	6.77	3.16	0.20	−2.09
TR	1.97	−3.11	4.43	7.19	0.24	1.16	1.39	−17.85	−0.22	−4.43	−0.46	−6.18	5.73	−33.54	0.21	7.99
AG	−5.33	−38.74	6.30	−18.23	−13.88	−40.23	−11.54	−46.83	−5.66	−24.92	−11.62	−32.10	−4.44	−60.72	−11.49	−20.84
LDI	2.24	−16.67	−2.33	−4.49	11.56	−3.95	8.81	−12.50	3.16	−9.68	9.33	−3.95	1.72	−22.22	12.60	7.35
RV	−9.28	−25.79	0.15	−16.48	−10.13	−15.97	1.29	−7.29	0.69	−5.22	−12.32	−18.10	−3.28	−16.92	−2.39	−3.12
LRVI	−12.36	−29.03	−1.90	−21.31	−15.11	−24.09	−2.77	−14.62	−1.90	−10.88	−15.38	−19.71	−7.30	−23.53	−6.63	−9.38
HVI	4.57	−23.64	14.86	−2.99	−1.79	−29.03	−0.22	−43.75	1.94	−11.86	−1.38	−25.00	5.75	−53.33	0.22	−14.29
VLD	16.17	5.97	25.00	21.48	11.76	4.65	12.83	−5.95	10.78	10.17	10.20	4.85	20.84	−5.88	9.47	16.46

(12.23%), and *Q. variabilis* (3.86%) were more broadly represented.

In the 5-m radius units the Cluster D captured more structurally diverse forests with higher vertical irregularity than Clusters B and C. It demonstrated elevated diversity metrics (RV: 2.449; LRVI: 0.749; HVI: 0.531; VLD: 0.651) along with moderate values for AG (5.092) and LDI (0.432) values (Table 4). These patterns indicate a higher level of species and structural heterogeneity, making it as transitional between the intermediate and highly complex forest types. Cluster D comprised 9454 analytical units, with a dominant representation from *Q. mongolica* (55.17%) and a relatively even distribution among other species, indicating a diverse species compositions (Table 5). Cluster D represented 14.2% of 5-m units, while its analogous Cluster C in the 10-m radius units comprised 11.3% of the total, reflecting similar layering complexity and forming the upper-middle complexity range (Fig. 5(b3)).

Clusters E (5-m radius unit) and D (10-m radius unit) exhibited the most structurally complex and vertically irregular forest stands, characterized by the highest RV (5-m E: 4.114; 10-m D: 4.112), LRVI (5-m E: 1.324; 10-m D: 1.333), and HVI (5-m E: 0.559; 10-m D: 0.612) values among all clusters (Table 4). These indicators suggest not only substantial differences in layer thickness but also highly uneven layer distribution—conditions typical of mixed-species, late-successional forests. AG values were also the highest (5-m E: 5.287; 10-m D: 6.266; Table 4), indicating sparse but deep stratification and layer diversification. Cluster E accounted for only 4.5% of 5-m units, while its 10-m counterpart (Cluster D) accounted for 5.9%, highlighting that such highly complex stands are relatively rare in the landscape (Figs. 4(b5) and 5(b4)). These clusters had the lowest LDI values (5-m E: 0.379; 10-m D: 0.323), highlighting lower layer compactness resulting from increased vertical separation. The absence of Cluster E at 10-m radius unit reflects scale-dependent integration of structural heterogeneity. Larger units merge fine-scale irregularities and transitional patches into neighboring types, reducing distinguishable clusters.

The noise groups were identified in both 5- and 10-m analytical units. They accounted for 4.9% and 11.2% of total units, respectively, indicating that a larger analytical radius tends to incorporate more heterogeneous plots into the unclassified category. These groups showed high RV values (5-m: 3.036; 10-m: 2.246) and moderate VLD (5-m: 0.692; 10-m: 0.668), suggesting internally variable but ecologically relevant variation that did not align with any specific clusters (Table 4).

5. Discussions

5.1. Methodological advances in forest vertical layer analysis

The precise segmentation of vertical forest layers is fundamental for detailed structural analysis. Building upon the histogram and derivative-based approach developed by Hamraz et al. (2017), our systematic evaluation of 54 parameter combinations (Table 1) identified optimal settings (1.0 m ground filtering, 1.0 m histogram bin size & Gaussian kernel, and 0.25–0.5 m voxelization). These settings significantly minimized errors (MAE $\approx$ 0.4) when compared to expert field investigations. This rigorous optimization reinforces the principle that LiDAR-derived products are highly sensitive to processing choices (Zhang et al., 2017; Wernicke et al., 2022). While Zhang et al. (2017) highlighted the impact of voxel size on subsequent canopy metric estimation, Wernicke et al. (2022) further emphasized the methodological challenges in accurately classifying forest strata, demonstrating that the selection of input metrics and classification algorithms significantly affects stratification accuracy. Our study directly addresses this challenge by providing specific, empirically validated parameters for the layer segmentation process, thereby offering a replicable foundation for subsequent structural quantification. The high accuracy achieved validates the utility of the modified Hamraz et al. (2017) method for Korean temperate forests, presenting a more objective alternative to traditional field surveys, which can be subjective and labor-intensive (Zimble et al., 2003).

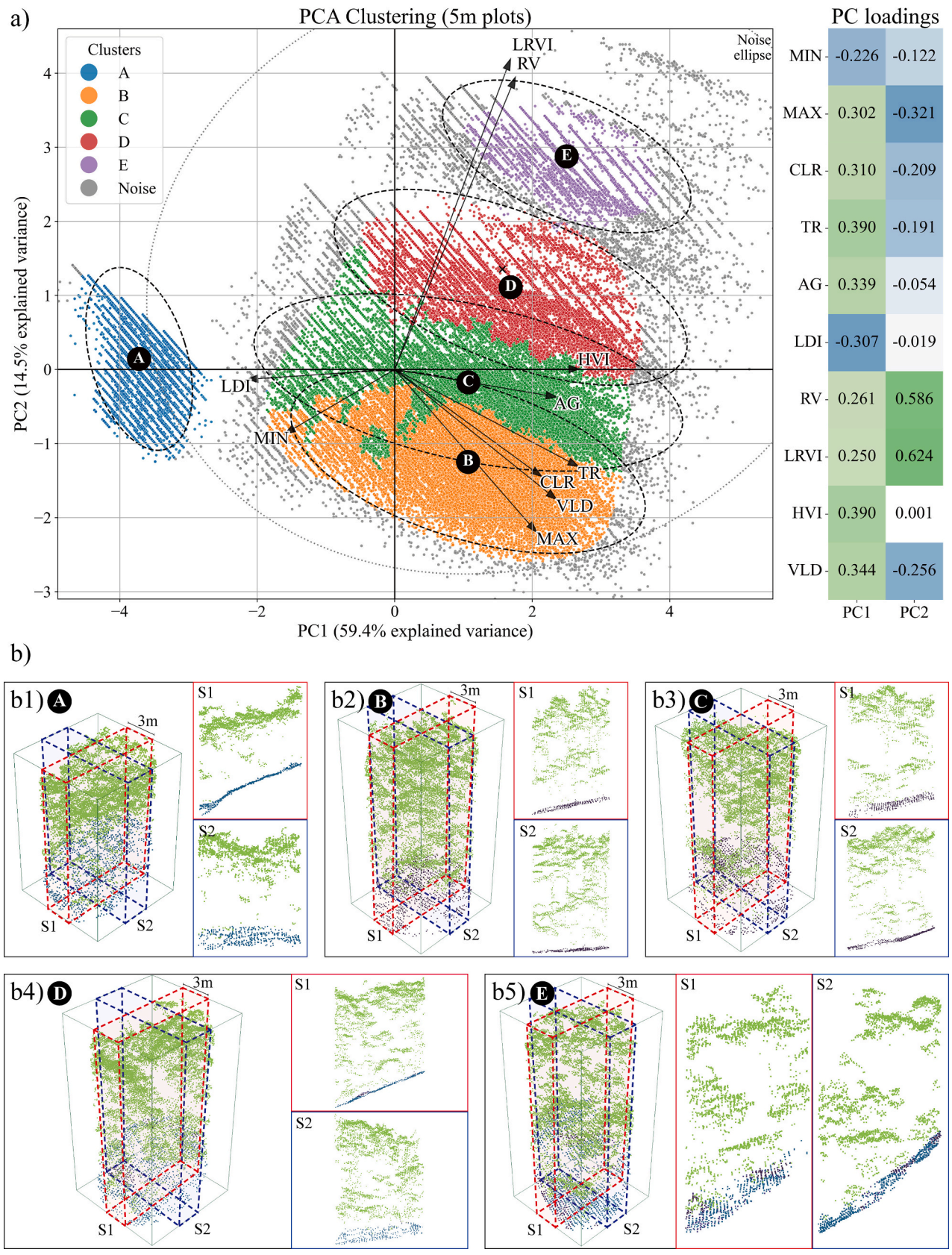

Fig. 4. PCA–HDBSCAN clustering results for 5-m radius analytical units. (a) PCA visualization of ten indices with explained variance on PC1 and PC2. Five clusters (A–E) and noise points (gray) are shown, with loading vectors displayed as a heatmap; (b) Point cloud examples for clusters A–E (b1–b5) with cross-sectional views with 3 m width (S1, S2).

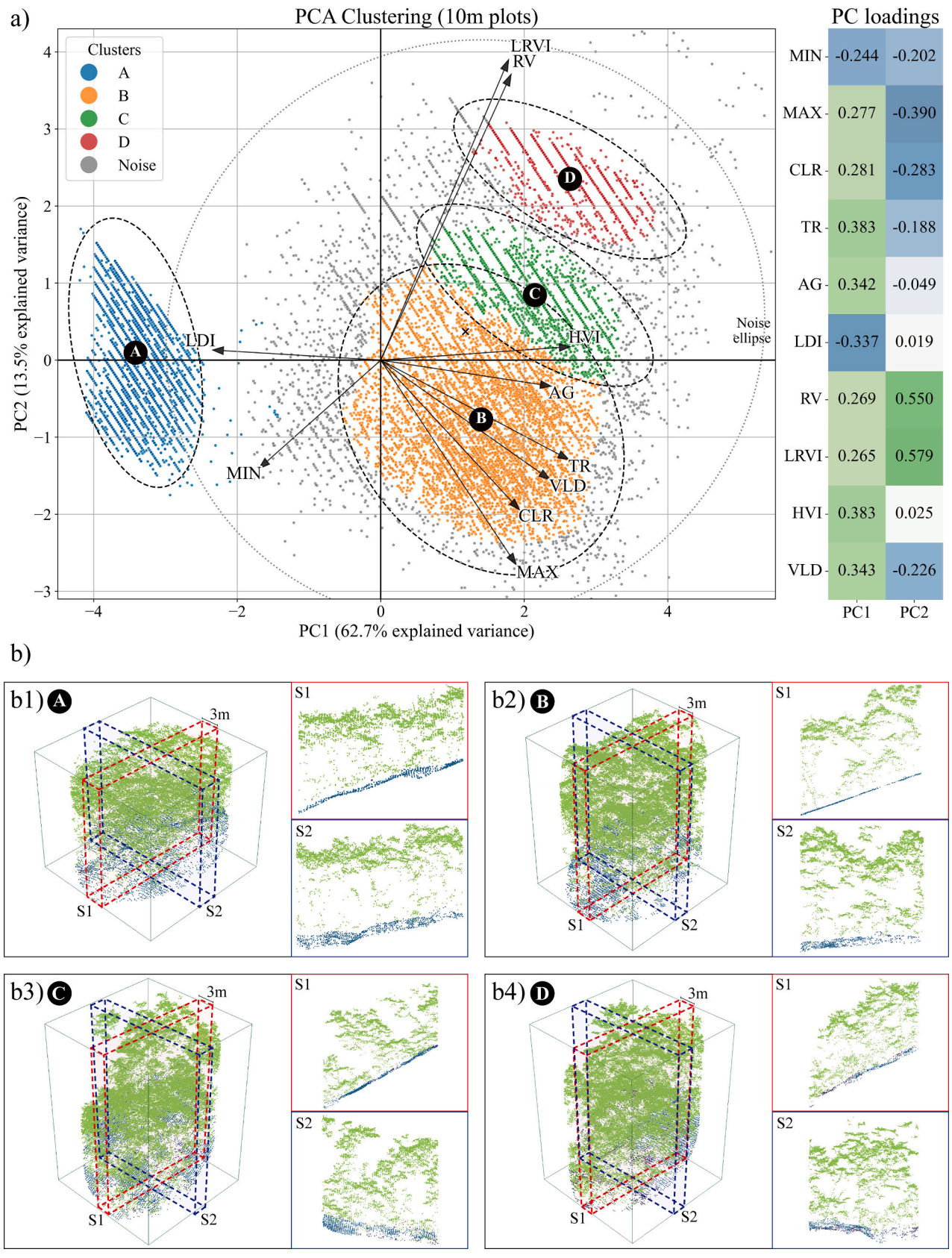

Fig. 5. PCA–HDBSCAN clustering results for 10-m radius analytical units. (a) PCA visualization of ten indices with explained variance on PC1 and PC2. Four clusters (A–D) and noise points (gray) are shown, with loading vectors displayed as a heatmap; (b) Point cloud examples for clusters A–D (b1–b4) with cross-sectional views with 3 m width (S1, S2).

Table 4
Average values of ten indices by unit size and cluster type.

Unit size		5-m radius analytical unit									
Indices		MIN	MAX	CLR	TR	AG	LDI	RV	LRVI	HVI	VLD
Clusters	A	6.245	12.466	4.269	4.269	0.000	1.000	0.000	0.000	0.000	0.000
	B	3.878	19.145	7.769	13.937	4.623	0.520	0.467	0.127	0.462	0.844
	C	3.382	17.550	6.931	12.885	4.560	0.502	1.237	0.358	0.493	0.762
	D	3.169	17.371	6.946	13.021	5.092	0.432	2.449	0.749	0.531	0.651
	E	2.891	17.100	7.384	13.032	5.287	0.379	4.114	1.324	0.559	0.545
	Noise	4.267	18.496	7.936	13.144	3.622	0.625	3.036	0.893	0.438	0.692
Unit size		10-m radius analytical unit									
Indices		MIN	MAX	CLR	TR	AG	LDI	RV	LRVI	HVI	VLD
Clusters	A	6.878	14.604	4.662	4.665	0.003	1.000	0.001	0.000	0.001	0.002
	B	3.545	20.035	7.515	14.084	5.429	0.420	0.979	0.290	0.502	0.759
	C	2.631	19.191	6.815	14.206	6.546	0.345	2.551	0.790	0.600	0.628
	D	2.403	18.499	7.008	13.546	6.266	0.323	4.112	1.333	0.612	0.520
	Noise	4.584	19.649	7.508	12.538	4.043	0.543	2.246	0.685	0.426	0.668

Table 5
Number and ratio of units in clusters for eight main species by unit size, including proportion of cluster units in the total dataset.

unit size			5-m radius analytical unit								
Species			*Quercus mongolica*	*Pinus densiflora*	*Castanea crenata*	*Quercus aliena*	*Pinus rigida*	*Quercus acutissima*	*Quercus variabilis*	*Pinus koraiensis*	Ratio of cluster units from entire units
Clusters	A	# of units	14,574	11,838	679	707	2,381	743	170	240	26.02%
		ratio in cluster	46.51%	37.78%	2.17%	2.26%	7.60%	2.37%	0.54%	0.77%	
	B	# of units	17,159	2,782	3,804	3,650	2,225	2,814	1,096	542	28.30%
		ratio in cluster	50.36%	8.17%	11.16%	10.71%	6.53%	8.26%	3.22%	1.59%	
	C	# of units	14,184	3,264	2,243	2,246	1,886	1,606	607	457	22.00%
		ratio in cluster	53.54%	12.32%	8.47%	8.48%	7.12%	6.06%	2.29%	1.72%	
	D	# of units	9,454	2,232	1,214	1,302	1,302	947	377	309	14.23%
		ratio in cluster	55.17%	13.02%	7.08%	7.60%	7.60%	5.53%	2.20%	1.80%	
	E	# of units	3,306	698	337	321	368	241	79	112	4.54%
		ratio in cluster	60.53%	12.78%	6.17%	5.88%	6.74%	4.41%	1.45%	2.05%	
	noise	# of units	3,079	755	541	436	367	518	136	76	4.91%
		ratio in cluster	52.12%	12.78%	9.16%	7.38%	6.21%	8.77%	2.30%	1.29%	
Unit size			10-m radius analytical unit								
Species			*Quercus mongolica*	*Pinus densiflora*	*Castanea crenata*	*Quercus aliena*	*Pinus rigida*	*Quercus acutissima*	*Quercus variabilis*	*Pinus koraiensis*	ratio of cluster units from entire units
Clusters	A	# of units	2,863	1,862	141	196	402	169	35	46	31.81%
		ratio in cluster	50.11%	32.59%	2.47%	3.43%	7.04%	2.96%	0.61%	0.81%	
	B	# of units	3,498	519	737	874	520	645	276	77	39.79%
		ratio in cluster	48.95%	7.26%	10.31%	12.23%	7.28%	9.03%	3.86%	1.08%	
	C	# of units	1,139	200	157	188	125	144	46	28	11.29%
		ratio in cluster	56.19%	9.87%	7.75%	9.27%	6.17%	7.10%	2.27%	1.38%	
	D	# of units	666	127	61	58	66	46	20	18	5.91%
		ratio in cluster	62.71%	11.96%	5.74%	5.46%	6.21%	4.33%	1.88%	1.69%	
	noise	# of units	1,085	205	159	153	146	199	50	15	11.20%
		ratio in cluster	53.93%	10.19%	7.90%	7.60%	7.26%	9.89%	2.49%	0.75%	

5.2. Ecological insights from novel vertical layer indices: Species-specificity and scale dependency

The ten vertical layer indices were used in this study, categorized into layer height, gap, and diversity, provide a multifaceted quantification of vertical structure. This analysis reveals significant species-specific traits and sensitivities to different analytical scales (5- and 10-m radii analytical units, Table 3).

5.2.1. Layer height indices: delineating vertical extent and development

Layer height indices provide fundamental information on the vertical extent and overall development of forest canopies. The MIN index, which represents understory initiation, exhibited minimal interspecific variation (typically 4-5 m across species in 5-m radius unit), but was notably sensitive to scale for *Q. variabilis* (22.26% decreased from 5- and 10-m radii analytical units). This scale sensitivity in the MIN suggests that the detection of lower canopy elements, which are crucial for understory characterization (Sasaki et al., 2012; Song et al., 2021), can be

significantly influenced by unit radius, possibly due to edge effects or the inclusion of more varied ground topography in larger units. This finding is further supported by the research of Yip et al. (2024) on the effects of sampling geometry on vertical range measurements.

The CLR and TR indices provide distinct insights into vertical layer. CLR, which sums the actual ranges of layers, represents the developed foliage space, while TR captures the overall vertical niche, including inter-layer gaps. As a result, TR values in our study were approximately 50% larger than CLR values. The CLR demonstrated remarkable consistency across unit scales (delta ratio $< \pm 3.50\%$) except *Q. variabilis*, underscoring its robustness as an indicator of foliage development, regardless of minor changes in unit sizes. This stability makes CLR a promising metric for comparative studies and upscaling efforts. Additionally, CLR conceptually aligns with the 'filled' voxel approach of the Canopy Volume Model (CVM) proposed by Zhang et al. (2017), which differentiates between vegetated and void spaces. However, unlike CVM, our CLR further quantifies the actual developed vertical layers and directly provides the summed range of these layers.

These layer height indices are fundamental for quantifying the vertical structure of a forest, which is directly linked to productivity and forest dynamics. MAX and TR serve as direct structural indicators highly correlated with essential forest inventory attributes such as Aboveground Biomass and wood volume in various forest types (Pan et al., 2011; Fayad et al., 2014; Zhang et al., 2017). The MIN index is critical for ecological applications focused on the understory, as it defines the starting point of lower canopy elements, which is essential for assessing understory light competition, resource allocation, and regeneration dynamics (Song et al., 2021; Royo and Carson, 2006). Furthermore, the CLR, which measures the aggregated vertical space occupied by foliage, functions as a robust proxy for total vertical foliage development. Its capacity for scale-invariant estimation makes it highly valuable for applying the Area-Based Approach in large-area biomass and carbon mapping (White et al., 2016; Wulder et al., 2012).

5.2.2. Layer gap indices: quantifying vertical porosity and compactness

Our layer gap indices, AG and LDI, provide critical insights into vertical layer porosity and compactness, which influence light regimes and habitat availability (Parker, 1995). The AG, specifically measures the mean vertical voids between identified layers and aligns with the Vertical Gap Index (VGI) developed by Jung et al. (2013) to quantify the amount of vertical open space using LiDAR. AG increased in larger units for every species except *P. densiflora*, with notable increases for *C. crenata* and *Q. acutissima* (13.88% and 11.62%, respectively), reflecting an enhanced capture of vertical voids with larger spatial range. These results confirm the importance of observation scale as a critical factor in gap detection (Gaulton and Malthus, 2010; Liu et al., 2018), thereby highlighting the need for careful consideration of scale when interpreting such metrics.

The LDI, inversely related to AG, effectively quantifies structural compactness. Coniferous species such as *P. densiflora*, with LDI values of 0.77 and 0.79 in 5- and 10-m radii analytical units respectively, exhibited the highest LDI values. This reflects their dense, compact vertical structures with minimal inter-layer voids. This finding is consistent with the general understanding of conifer architecture and is conceptually similar to studies that utilize return density as a proxy for vertical compaction (Martins-Neto et al., 2021). LDI offers novel characterizations of layer density, complementing traditional metrics that focus on overall canopy openness (Sasaki et al., 2016; Kwak et al., 2010) by detailing the internal arrangement of vegetated layers rather than just total void space. Furthermore, the LDI enhances analyses of larger horizontal clearings (Gaulton and Malthus, 2010; Choi et al., 2019) by characterizing layer compactness within internal vertical structures.

The layer gap indices are essential for quantifying the canopy's internal porosity and density, which govern light and energy transfer, thereby regulating the sub-canopy microclimate and species distribution (Parker, 1995; Parker and Brown, 2000). The AG index measures vertical openness, reflecting structural fragmentation and aligning with metrics like the Deep Gap Fraction used to estimate light penetration and LAI based on the Beer–Lambert Law (Atkins et al., 2018a,b; Zhao et al., 2012). This metric is crucial for analyzing gap regeneration dynamics (Spies and Franklin, 1989) and assessing disturbance regimes (Johnstone et al., 2016). In contrast, the LDI quantifies structural compactness. High compactness (low vertical void space) is ecologically significant as it enhances localized habitat availability and improves the forest's microclimate buffering capacity, which is crucial for managing forest ecosystems in the face of climate change (De Frenne et al., 2021; Zellweger et al., 2020).

5.2.3. Layer diversity index: capturing vertical heterogeneity

The layer diversity indices (RV, LRVI, HVI, VLD) encapsulate vertical heterogeneity, a key component of forest structural complexity that is often linked to biodiversity and ecosystem stability (Jucker et al., 2014). RV and LRVI quantify variability in the thickness of identified layers, revealing significant structural variation in species like *Q. variabilis* (RV 1.31, LRVI 0.40 at 5-m) and *Q. acutissima* (RV 1.27, LRVI 0.36 at 5-m). This indicates complex foliage layering and diverse growth forms, providing a more specified perspective on complex foliage layering than general canopy height variance metrics (Zimble et al., 2003). Furthermore, these indices demonstrated scale sensitivity, as evidenced by *Q. acutissima* RV and LRVI, respectively showing a delta of −12.32% and − 15.38%. This finding is consistent with finer analytical units can detect greater intra-structural detail (Ma et al., 2022).

The VLD, adapted in our study from the proportions of layer height ranges, provides a robust measure of vertical stratification complexity. This approach aligns with numerous recent studies that employ LiDAR-derived entropy-based or Shannon-like indices to characterize forest structure and its relationship to species diversity (Ren et al., 2023; Liu et al., 2022; Yip et al., 2024; Hirschmugl et al., 2023). However, our HVI and VLD also revealed a more pronounced scale dependency than anticipated, with delta ratios reaching up to 25% for VLD in *P. densiflora* and significant changes observed for *Q. variabilis* (VLD decreased from 0.64 to 0.51). This indicates that the observed vertical diversity is significantly influenced by spatial resolution, which aligns with cautions regarding the interpretation of multi-scale data (Ren et al., 2023; Liu et al., 2022) and underscores the importance of proper scale setting for ecological assessments.

These indices are critical for assessing Vertical Structural Complexity (VSC), a parameter widely accepted as a strong predictor of biodiversity, ecosystem stability, and function (Shugart et al., 2010; Hardiman et al., 2011; LaRue et al., 2023). VSC is directly related to ecosystem stability, resilience to disturbance (Johnstone et al., 2016) and high carbon storage potential (Aponte et al., 2020). Moreover, the capacity of VLD and LRVI to capture the fine-scale variability and irregularity of layer placement enables the identification and monitoring of the complex, multi-tiered architectures characteristic of mature or late-successional forests (Kane et al., 2010; Ehbrecht et al., 2021). These entropy-based indices are demonstrably superior to traditional height metrics for monitoring forest restoration success and modeling diversity across large, diverse landscapes (Liu et al., 2022).

5.3. Ecological interpretation of structural typologies from PCA-HDBSCAN and scale effects

In this section, we discuss the structural typologies identified by PCA–HDBSCAN using ten vertical layer indices. PCA was used to derive the feature space for clustering, while typologies are interpreted using cluster-wise summaries of the original indices. The PCA-HDBSCAN stratified the analytical units into four distinct vertical structural types at the 10-m radius unit and five types at the 5-m radius unit, along with a noise cluster at both scales (Figs. 4 and 5; Tables 4 and 5). This data-driven framework summarized the heterogeneous vertical structural variation in the analytical units, with PC1 and PC2 together explaining

over 70% of the variance in the index set. PCA has been used in forest-structure studies to summarize LiDAR-derived structural metrics prior to downstream analyses (Alexander et al., 2018). HDBSCAN was then applied to identify groups in the reduced feature space without pre-defining the number of clusters, while allowing structurally ambiguous units to be labeled as noise. Similar unsupervised workflows have been used in LiDAR-based studies, such as tree stem segmentation (Neuville et al., 2021) and forest structure classification using LiDAR-derived L-moments without pre-defined thresholds (Moran et al., 2018). Our resulting clusters can be conceptualized as empirically derived "structural fingerprints," as termed by Gonçalves et al. (2024) in their study of Amazonian forests using LiDAR and deep learning. These fingerprints represent a continuum of forest structural states, ranging from simple monolayers to vertically complex stands, each characterized by distinct combinations of our ten vertical layer indices (Table 4). Cluster-wise differences in dominant species composition (Table 5) are presented as descriptive patterns that co-occur with the structural typologies.

Cluster A, consistently identified at both the 5- and 10-m radii units, represented the simplest vertical structures. This cluster was characterized by the lowest vertical development (MAX 5-m: 12.466 m, CLR 5-m: 4.269 m), the absence of inter-layer gaps (AG $\approx$ 0), perfect compactness (LDI $\approx$ 1.0), and minimal diversity across all layer diversity indices (RV, LRVI, HVI, VLD all near zero). Dominated by coniferous species such as *P. densiflora* (37.78% of the Cluster A among 5-m radius units), this structural signature is consistent with descriptions of early-successional stands or managed, even-aged conifer plantations, which typically exhibit low structural complexity (White et al., 2013). Kane et al. (2010), in their examination of conifer canopy structural complexity using LiDAR across various forest ages and elevations in the Pacific Northwest, also identified low-complexity classes in younger or less developed stands characterized by uniform canopy heights and densities, showing comparable low-complexity features to our Cluster A. Similarly, Zhang et al. (2011), who classified cool temperate rainforests and adjacent eucalypt forests in Australia using airborne LiDAR, identified structurally simpler forest types such as "Low Open Forest" and certain "Eucalypt Forest" classes that, based on their descriptions of lower canopy height and simpler structure, are broadly consistent with such single-layered, dense canopies.

Clusters B and C at the 5-m scale, which largely merged into a broader Cluster B at the 10-m scale, represented intermediate structural complexity with moderate values across most indices. This indicates partially stratified canopies with a mixed species composition. The amalgamation of finer-scale distinctions (5-m Clusters B and C) into a more generalized cluster at the 10-m scale illustrates how increasing the analytical unit size can average out localized heterogeneity, potentially obscuring subtle variations that are important for niche differentiation or microhabitat availability. This observation aligns with Zhao et al. (2011), who noted that while composite LiDAR metrics are useful for characterizing overall structure, very large observation footprints can average out fine-scale details. Similarly, at the 10-m scale, Cluster E is absent because coarser analytical footprints aggregate micro-structural variation and edge mosaics into broader canopy categories, thereby diminishing cluster distinctness. Importantly, this scale-driven reduction in cluster number arises from spatial aggregation rather than differences in the number of analytical units, as both datasets represent the same forest area sampled at different resolutions. These intermediate clusters show a mixed coniferous-broadleaf composition. *Q. mongolica* is prominent but less dominant than in the more complex types, and *C. crenata* and *Q. aliena* are also notable in the 10-m Cluster B (Table 5). This species pattern is observed alongside the transitional, mixed structural profile of these clusters.

The 5-m Cluster D and its 10-m counterpart Cluster C, exhibited upper-middle complexity. These clusters were characterized by elevated layer diversity indices (e.g., at 5-m, Cluster D had RV = 2.449, LRVI = 0.749, VLD = 0.651) and moderate AG (5.092 m) (Table 4). These characteristics are indicative of active mid-to-late successional stands, which are often associated with increased species diversity and biomass accumulation, as demonstrated by Almeida et al. (2020), who utilized drone LiDAR to monitor successional changes in tropical forest structure. Furthermore, the findings of Jucker et al. (2014) indicate that structurally and species-diverse forest stands can sustain ecosystem functions such as productivity and provide resilience against structural shifts. Overall, these clusters represent intermediate-to-high structural complexity. The framework proposed by Atkins et al. (2018a,b) for quantifying canopy structural complexity, although based on terrestrial LiDAR, emphasizes metrics like FHD and the number of layers; higher values for these metrics would correspond with the characteristics of the more developed forest stages identified in our study.

The most complex structural types, Clusters E (at 5-m scale) and D (at 10-m scale), exhibited the highest values for diversity indices (e.g., 5-m Cluster E: RV = 4.114, LRVI = 1.324, HVI = 0.559) and gap index (AG = 5.287 m), along with the lowest LDI (0.379) (Table 4). These characteristics are indicative of late-successional, mature, mixed-species forests and are often associated with long-term ecological processes (Jung et al., 2013; Svenning et al., 2004). Similarly, Hilker et al. (2009), while mapping forest disturbances, implicitly demonstrated that undisturbed or later successional areas typically exhibit greater structural complexity, which can be captured through remote sensing. The high AG and low LDI values indicate significant vertical differentiation and internal openness, which are crucial for maintaining diverse light environments within the canopy and providing varied habitats.

Finally, the 'noise' cluster identified by HDBSCAN in both the 5- and 10-m radii units analyses likely represents ecologically meaningful yet structurally ambiguous units (e.g., transitional or edge areas) rather than mere analytical errors. These units exhibited high RV values but moderate VLD, indicating internal structural variability that deviates from the dominant patterns of the other clusters. The higher proportion of noise at the 10-m scale (11.2%; 4.9% at 5-m scale) reflects a scale-dependent smoothing effect, where larger analytical units merge contrasting micro-structures -such as local canopy gaps or mixed stands- into unclassified plots. In addition, a 0.5-m resolution DEM based analysis confirmed no significant relationship between noise distribution and topographic factors (elevation or slope), suggesting that their occurrence arises from intrinsic fine-scale heterogeneity rather than terrain influence. Ecologically, these 'noise' units represent structural mosaics or ecotonal zones characterized by ongoing canopy adjustment and spatial heterogeneity. The ability of HDBSCAN to isolate such ambiguous structures as 'noise', rather than forcing them into ill-fitting groups, remains a key advantage in complex ecological datasets (Neuville et al., 2021). This finding aligns with previous LiDAR studies noting the challenge of discretely classifying diverse forest structures (Moran et al., 2018).

5.4. Research limitations and future works

While this study established a robust methodological framework for quantifying forest vertical structure using novel indices and ecologically interpretable typologies in Korean temperate forests, its limitations underscore several key avenues for future research. The findings, including optimal parameters and index sensitivities, are currently specific to the temperate mixed forest at our study site and the characteristics of the ALS data. Future work must assess the generalizability of these findings across diverse forest biomes (such as tropical, boreal, and other temperate systems), different LiDAR sensors, and varying point densities (Hirschmugl et al., 2023). The visual field validation of layer numbers, although expert-driven, could be improved by incorporating quantitative terrestrial LiDAR measurements for ground-truthing canopy layering and foliage profiles, following methodologies similar to those proposed by Atkins et al. (2018a,b). Additionally, expanding the species-specific analysis beyond the eight dominant species is warranted. It is also important the unbalanced number of units among

species, a result of the natural distribution in the study site, may influence the statistical robustness for lowerly distributed species. Furthermore, the adapted layer definition method from Hamraz et al. (2017) represents just one of several possibilities; comparative studies utilizing alternative techniques, such as mixture models (Jaskierniak et al., 2011) or different segmentation algorithms, could provide further insights into optimizing the characterization of vertical structure.

Building on these limitations, future research should prioritize enhancing ecological validation and functional linkages. This involves directly correlating our structural indices and typologies with field-measured biodiversity (Yip et al., 2024; Ren et al., 2023), microclimatic conditions and essential ecosystem functions, including forest productivity, nutrient cycling, and carbon sequestration. The "structural fingerprints" approach proposed by Gonçalves et al. (2024), which connects LiDAR-derived structural data to topographical influences and potential ecosystem functions, offers a promising model. Furthermore, our indices could contribute to other process models, such as canopy fuel loading (Skowronski et al., 2011). Exploring spatio-temporal dynamics and upscaling capabilities is another critical area of research. Multi-temporal LiDAR datasets can reveal successional pathways and responses to disturbances (Choi et al., 2019). Integrating our detailed ALS-derived metrics derived from ALS with data from other sensors, such as spaceborne LiDAR (GEDI, ICESat/GLAS) (Ren et al., 2023; Hirschmugl et al., 2023; Fayad et al., 2014) or multispectral and hyperspectral imagery (Wilkes et al., 2015; Wernicke et al., 2022), is key for comprehensive landscape assessments. Addressing these limitations and pursuing future research directions will significantly enhance the utility of LiDAR-derived vertical structure information, thereby advancing forest ecology and supporting evidence-based sustainable forest management on a global scaled.

6. Conclusion

This study established an optimized forest layer segmentation protocol and introduced a multi-scale, multi-index approach for the detailed assessment and clustering of forest vertical layers using high-density ALS data. The results yielded three key findings. First, the ten vertical layer indices demonstrated high fidelity in capturing species-specific structural characteristics, effectively distinguishing the heterogeneous complexity of broadleaved canopies from the more homogeneous forms of coniferous stands. Second, the multi-scale comparison revealed statistically significant scale dependencies across both species and indices; for example, layer diversity measures, particularly VLD, were closely associated with the spatial extent of the analysis. Third, the PCA–HDBSCAN unsupervised clustering approach successfully stratified the landscape into ecologically interpretable structural typologies, revealing a clear gradient from simple monolayer stands to structurally complex, late-successional systems. In synthesizing these findings, this research provides an empirically validated toolkit for multi-faceted structural assessment and establishes a robust, quantitative foundation for future investigations into structure–function relationships, biodiversity modeling, and the development of evidence-based strategies for sustainable forest management.

Beyond methodological advancement, the ten vertical layer indices proposed here provide functional ecological value for forest monitoring and management. Height-based indices can be applied to evaluate stand development and biomass accumulation. Gap-related indices quantify the vertical separation between adjacent canopy layers (inter-layer gaps), informing assessments of within-canopy light environments, understory habitat conditions, and the degree of vertical compactness. Diversity indices capture internal structural heterogeneity relevant to resilience evaluation, restoration progress, and ecological complexity. Collectively, these indices provide a scalable framework linking LiDAR-derived structure to practical applications in forest conservation, biodiversity assessment, and policy-oriented ecosystem management.

CRediT authorship contribution statement

Seunghyeon Lee: Writing – review & editing, Writing – original draft, Visualization, Validation, Software, Methodology, Investigation, Formal analysis, Conceptualization. **Uirin Ha:** Writing – original draft, Methodology, Conceptualization. **Heejae Lee:** Writing – review & editing, Writing – original draft, Methodology, Investigation, Conceptualization. **Hyeyeong Choe:** Writing – review & editing, Conceptualization. **Hansoo Kim:** Writing – review & editing, Project administration, Data curation, Conceptualization. **Youngkeun Song:** Writing – review & editing, Supervision, Project administration, Funding acquisition, Data curation, Conceptualization.

Declaration of competing interest

The authors declare that they have no known competing financial interests or personal relationships that could have appeared to influence the work reported in this paper.

Acknowledgements

This work was supported by Korea Environment Industry & Technology Institute(KEITI) through Technology Development Project for Creation and Management of Ecosystem based Carbon Sinks, funded by Korea Ministry of Climate, Energy and Environment(MCEE) (RS-2023–00218245) And this study was supported by the [Gyeonggi-do Metropolitan Biotope Map Establishment Planning Study]. And This work is financially supported by Korea Ministry of Land, Infrastructure and Transport (MOLIT) as 「Innovative Talent Education Program for Smart City」. And this work was supported by the Hyundai Motor Chung Mong-Koo Foundation.

Appendix A. Supplementary data

Supplementary data to this article can be found online at https://doi.org/10.1016/j.ecolind.2026.114798.

Data availability

The data that has been used is confidential.

References

Alexander, Cici, Korstjens, Amanda H., Usher, Graham, Nowak, Matthew G., Fredriksson, Gabriella, Hill, Ross A., 2018. LiDAR Patch metrics for object-based clustering of Forest types in a tropical rainforest. Int. J. Appl. Earth Obs. Geoinf. 73, 253–261.

Almeida, Danilo Roberti Alves de, Almeyda Zambrano, Angelica Maria, Broadbent, Eben North, Wendt, Amanda L., Foster, Paul, Wilkinson, Benjamin E., Salk, Carl, de Almeida Papa, Daniel, Stark, Scott Christopher, Valbuena, Ruben, 2020. Detecting successional changes in tropical forest structure using GatorEye drone-borne Lidar. Biotropica 52 (6), 1155–1167.

Aponte, C., Kasel, S., Nitschke, C.R., Tanase, M.A., Vickers, H., Parker, L., Bennett, L.T., 2020. Structural diversity underpins carbon storage in Australian temperate forests. Global Ecology and Biogeography 29 (5), 789–802.

Atkins, J.W., Fahey, R.T., Hardiman, B.S., Gough, C.M., 2018a. Forest canopy structural complexity and light absorption relationships at the subcontinental scale. J. Geophys. Res. Biogeosci. 123 (4), 1387–1405.

Atkins, Jeff W., Bohrer, Gil, Fahey, Robert T., Hardiman, Brady S., Morin, Timothy H., Stovall, Atticus E.L., Zimmerman, Naupaka, Gough, Christopher M., 2018b. Quantifying vegetation and canopy structural complexity from terrestrial Li DAR data using the Forestr r package. Methods Ecol. Evol. 9 (10), 2057–2066.

Choi, Heejoon, Song, Youngkeun, Jang, Youngwoon, 2019. Urban forest growth and gap dynamics detected by yearly repeated airborne light detection and ranging (LiDAR): a case study of Cheonan, South Korea. Remote Sens. 11 (13), 1551.

Deng, Jiaojiao, Fang, Shuai, Fang, Xiangmin, Jin, Yanqiang, Kuang, Yuanwen, Lin, Fangmei, Liu, Jiaqing, Ma, Jingran, Nie, Yanxia, Ouyang, Shengnan, 2023. Forest understory vegetation study: current status and future trends. Forest. Res. 3, 6.

Ehbrecht, Martin, Schall, Peter, Ammer, Christian, Seidel, Dominik, 2017. Quantifying stand structural complexity and its relationship with Forest management, tree species diversity and microclimate. Agric. For. Meteorol. 242, 1–9.

Ehbrecht, Martin, Seidel, Dominik, Annighöfer, Peter, Kreft, Holger, Köhler, Michael, Zemp, Delphine Clara, Puettmann, Klaus, Nilus, Reuben, Babweteera, Fred, Willim, Katharina, 2021. Global patterns and climatic controls of forest structural complexity. Nat. Commun. 12 (1), 519.
Fayad, Ibrahim, Baghdadi, Nicolas, Bailly, Jean-Stéphane, Barbier, Nicolas, Gond, Valéry, El Hajj, Mahmoud, Fabre, Frédéric, Bourgine, Bernard, 2014. Canopy height estimation in French Guiana with LiDAR ICESat/GLAS data using principal component analysis and random Forest regressions. Remote Sens. 6 (12), 11883–11914.
Féret, J.B., Asner, G.P., 2012. Semi-supervised methods to identify individual crowns of lowland tropical canopy species using imaging spectroscopy and LiDAR. Remote Sensing 4 (8), 2457–2476.
Frazer, G.W., Magnussen, S., Wulder, M.A., Niemann, K.O., 2011. Simulated impact of sample plot size and co-registration error on the accuracy and uncertainty of LiDAR-derived estimates of Forest stand biomass. Remote Sens. Environ. 115 (2), 636–649.
Frenne, De, Pieter, Jonathan Lenoir, Luoto, Miska, Scheffers, Brett R., Zellweger, Florian, Aalto, Juha, Ashcroft, Michael B., Christiansen, Ditte M., Decocq, Guillaume, De Pauw, Karen, 2021. Forest microclimates and climate change: importance, drivers and future research agenda. Glob. Chang. Biol. 27 (11), 2279–2297.
Gaulton, Rachel, Malthus, Tim J., 2010. LiDAR mapping of canopy gaps in continuous cover forests: a comparison of canopy height model and point cloud based techniques. Int. J. Remote Sens. 31 (5), 1193–1211.
Gonçalves, Nathan Borges, Rosa, Diogo Martins, do Valle, Dalton Freitas, Smith, Marielle N., Dalagnol, Ricardo, de Almeida, Danilo Roberti Alves, Nelson, Bruce W., Stark, Scott C., 2024. Revealing forest structural" fingerprints": an integration of LiDAR and deep learning uncovers topographical influences on Central Amazon forests. Ecol. Inform. 81, 102628.
Hamraz, Hamid, Contreras, Marco A., Zhang, Jun, 2017. Forest understory trees can be segmented accurately within sufficiently dense airborne laser scanning point clouds. Sci. Rep. 7 (1), 6770.
Hardiman, Brady S., Bohrer, Gil, Gough, Christopher M., Vogel, Christoph S., Curtis, Peter S., 2011. The role of canopy structural complexity in wood net primary production of a maturing northern deciduous Forest. Ecology 92 (9), 1818–1827.
Hilker, Thomas, Wulder, Michael A., Coops, Nicholas C., Linke, Julia, McDermid, Greg, Masek, Jeffrey G., Gao, Feng, White, Joanne C., 2009. A new data fusion model for high spatial-and temporal-resolution mapping of Forest disturbance based on Landsat and MODIS. Remote Sens. Environ. 113 (8), 1613–1627.
Hirschmugl, Manuela, Lippl, Florian, Sobe, Carina, 2023. Assessing the vertical structure of forests using airborne and Spaceborne LiDAR data in the Austrian Alps. Remote Sens. 15 (3), 664.
Jaskierniak, Dominik, Lane, Patrick N.J., Robinson, Andrew, Lucieer, Arko, 2011. Extracting LiDAR indices to characterise multilayered Forest structure using mixture distribution functions. Remote Sens. Environ. 115 (2), 573–585.
Johnstone, Jill F., Allen, Craig D., Franklin, Jerry F., Frelich, Lee E., Harvey, Brian J., Higuera, Philip E., Mack, Michelle C., Meentemeyer, Ross K., Metz, Margaret R., Perry, George L.W., 2016. Changing disturbance regimes, ecological memory, and forest resilience. Front. Ecol. Environ. 14 (7), 369–378.
Jucker, Tommaso, Bouriaud, Olivier, Avacaritei, Daniel, Coomes, David A., 2014. Stabilizing effects of diversity on aboveground wood production in Forest ecosystems: linking patterns and processes. Ecol. Lett. 17 (12), 1560–1569.
Jucker, Tommaso, Bouriaud, Olivier, Coomes, David A., 2015. Crown plasticity enables trees to optimize canopy packing in mixed-species forests. Funct. Ecol. 29 (8), 1078–1086.
Jung, Jinha, Pekin, Burak K., Pijanowski, Bryan C., 2013. Mapping open space in an old-growth, secondary-growth, and selectively-logged tropical rainforest using discrete return LIDAR. IEEE J. Selected Topics Appl. Earth Observat. Remote Sens. 6 (6), 2453–2461.
Kane Van, R., Bakker, Jonathan D., McGaughey, Robert J., Lutz, James A., Gersonde, Rolf F., Franklin, Jerry F., 2010. Examining conifer canopy structural complexity across Forest ages and elevations with LiDAR data. Can. J. For. Res. 40 (4), 774–787.
Kwak, Doo-Ahn, Lee, Woo-Kyun, Kafatos, Menas, Son, Yowhan, Cho, Hyun-Kook, Lee, Seung-Ho, 2010. Estimation of effective plant area index for south Korean forests using LiDAR system. Sci. China Life Sci. 53 (7), 898–908.
LaRue, Elizabeth A., Fahey, Robert T., Alveshere, Brandon C., Atkins, Jeff W., Bhatt, Parth, Buma, Brian, Chen, Anping, Cousins, Stella, Elliott, Jessica M., Elmore, Andrew J., 2023. A theoretical framework for the ecological role of three-dimensional structural diversity. Front. Ecol. Environ. 21 (1), 4–13.
Lecigne, Bastien, Delagrange, Sylvain, Messier, Christian, 2018. Exploring trees in three dimensions: VoxR, a novel voxel-based R package dedicated to Analysing the complex arrangement of tree crowns. Ann. Bot. 121 (4), 589–601.
Lefsky, Michael A., Cohen, Warren B., Parker, Geoffrey G., Harding, David J., 2002. Lidar remote sensing for ecosystem studies: Lidar, an emerging remote sensing technology that directly measures the three-dimensional distribution of plant canopies, can accurately estimate vegetation structural attributes and should be of particular interest to Forest, landscape, and global ecologists. BioScience 52 (1), 19–30.
Liu, Jing, Skidmore, Andrew K., Jones, Simon, Wang, Tiejun, Heurich, Marco, Zhu, Xi, Shi, Yifang, 2018. Large off-nadir scan angle of airborne LiDAR can severely affect the estimates of Forest structure metrics. ISPRS J. Photogramm. Remote Sens. 136, 13–25.
Liu, Xiaoqiang, Ma, Qin, Wu, Xiaoyong, Hu, Tianyu, Liu, Zhonghua, Liu, Lingli, Guo, Qinghua, Su, Yanjun, 2022. A novel entropy-based method to quantify Forest canopy structural complexity from multiplatform Lidar point clouds. Remote Sens. Environ. 282, 113280.
Ma, Kaisen, Chen, Zhenxiong, Liyong, Fu, Tian, Wanli, Jiang, Fugen, Yi, Jing, Zhi, Du, Sun, Hua, 2022. Performance and sensitivity of individual tree segmentation methods for UAV-LiDAR in multiple Forest types. Remote Sens. 14 (2), 298.
MacArthur, Robert H., MacArthur, John W., 1961. On bird species diversity. Ecology 42 (3), 594–598.
Martins-Neto, Rorai Pereira, Tommaselli, Antonio Maria Garcia, Imai, Nilton Nobuhiro, David, Hassan Camil, Miltiadou, Milto, Honkavaara, Eija, 2021. Identification of Significative LiDAR metrics and comparison of machine learning approaches for estimating stand and diversity variables in heterogeneous Brazilian Atlantic Forest. Remote Sens. 13 (13), 2444.
McInnes, L., Healy, J., Astels, S., 2017. hdbscan: Hierarchical density based clustering. J. Open Source Softw. 2 (11), 205.
Montoya-Sánchez, Vannesa, Camarretta, Nicolo, Ehbrecht, Martin, Schlund, Michael, Paterno, Gustavo Brant, Seidel, Dominik, Guerrero-Ramírez, Nathaly, et al., 2024. Comparing airborne and terrestrial LiDAR with ground-based inventory metrics of vegetation structural complexity in oil palm agroforests. Ecol. Indic. 166, 112306.
Moran, Christopher J., Rowell, Eric M., Seielstad, Carl A., 2018. A data-driven framework to identify and compare Forest structure classes using LiDAR. Remote Sens. Environ. 211, 154–166.
Neuville, Romain, Bates, Jordan Steven, Jonard, François, 2021. Estimating Forest structure from UAV-mounted LiDAR point cloud using machine learning. Remote Sens. 13 (3), 352.
Oliver, Chadwick Dearing, Larson, Bruce C., Oliver, C.D., 1996. Forest Stand Dynamics, 520. Wiley, New York.
Ontl, Todd A., Janowiak, Maria K., Swanston, Christopher W., Daley, Jad, Handler, Stephen, Cornett, Meredith, Hagenbuch, Steve, Handrick, Cathy, Mccarthy, Liza, Patch, Nancy, 2020. Forest management for carbon sequestration and climate adaptation. J. For. 118 (1), 86–101.
Pan, Yude, Birdsey, Richard A., Fang, Jingyun, Houghton, Richard, Kauppi, Pekka E., Kurz, Werner A., Phillips, Oliver L., Shvidenko, Anatoly, Lewis, Simon L., Canadell, Josep G., 2011. A large and persistent carbon sink in the world's forests. Science 333 (6045), 988–993.
Parker, Geoffrey G., 1995. Structure and Microclimate of Forest Canopies.
Parker, Geoffrey G., Brown, Martin J., 2000. Forest canopy stratification—is it useful? Am. Nat. 155 (4), 473–484.
Ren, Chunying, Jiang, Hailing, Xi, Yanbiao, Liu, Pan, Li, Huiying, 2023. Quantifying temperate Forest diversity by integrating GEDI LiDAR and multi-temporal Sentinel-2 imagery. Remote Sens. 15 (2), 375.
Royo, Alejandro A., Carson, Walter P., 2006. On the formation of dense understory layers in forests worldwide: consequences and implications for Forest dynamics, biodiversity, and succession. Can. J. For. Res. 36 (6), 1345–1362.
Sasaki, Takeshi, Imanishi, Junichi, Fukui, Wataru, Tokunaga, Fukiko, Morimoto, Yukihiro, 2012. Fine-scale replication and quantitative assessment of Forest vertical structure using LiDAR for Forest avian habitat characterization. For. Sci. Technol. 8 (3), 145–153.
Sasaki, Takeshi, Imanishi, Junichi, Ioki, Keiko, Song, Youngkeun, Morimoto, Yukihiro, 2016. Estimation of leaf area index and gap fraction in two broad-leaved forests by using small-footprint airborne LiDAR. Landsc. Ecol. Eng. 12 (1), 117–127.
Seidel, Dominik, Fleck, Stefan, Leuschner, Christoph, Hammett, Tom, 2011. Review of ground-based methods to measure the distribution of biomass in Forest canopies. Ann. For. Sci. 68 (2), 225–244.
Shugart, H.H., Saatchi, S., Hall, F.G., 2010. Importance of structure and its measurement in quantifying function of forest ecosystems. J. Geophys. Res. Biogeosci. 115 (G2).
Skowronski, N.S., Clark, K.L., Duveneck, M., Hom, J., 2011. Three-dimensional canopy fuel loading predicted using upward and downward sensing LiDAR systems. Remote Sensing of Environment 115 (2), 703–714.
Song, Jinling, Zhu, Xiao, Qi, Jianbo, Pang, Yong, Yang, Lei, Yu, Lihong, 2021. A method for quantifying understory leaf area index in a temperate forest through combining small footprint full-waveform and point cloud LiDAR data. Remote Sens. 13 (15), 3036.
Spies, Thomas A., Franklin, Jerry F., 1989. Gap characteristics and vegetation response in coniferous forests of the Pacific northwest. Ecology 70 (3), 543–545.
Svenning, J.-C., Kinner, David A., Stallard, Robert F., Engelbrecht, Bettina M.J., Wright, S. Joseph, 2004. Ecological determinism in plant community structure across a tropical Forest landscape. Ecology 85 (9), 2526–2538.
Vonderach, C., Voegtle, T., Adler, P., 2012. Voxel-based approach for estimating urban tree volume from terrestrial laser scanning data. Int. Arch. Photogramm. Remote. Sens. Spat. Inf. Sci. 39, 451–456.
Wernicke, Jakob, Seltmann, Christian Torsten, Wenzel, Ralf, Becker, Carina, Körner, Michael, 2022. Forest canopy stratification based on fused, imbalanced and collinear LiDAR and Sentinel-2 metrics. Remote Sens. Environ. 279, 113134.
White, Joanne C., Wulder, Michael A., Varhola, Andrés, Vastaranta, Mikko, Coops, Nicholas C., Cook, Bruce D., Pitt, Doug, Woods, Murray, 2013. A best practices guide for generating Forest inventory attributes from airborne laser scanning data using an area-based approach. For. Chron. 89 (6), 722–723.
White, Joanne C., Coops, Nicholas C., Wulder, Michael A., Vastaranta, Mikko, Hilker, Thomas, Tompalski, Piotr, 2016. Remote sensing Technologies for Enhancing Forest Inventories: a review. Can. J. Remote. Sens. 42 (5), 619–641.
Wilkes, Phil, Jones, Simon D., Suarez, Lola, Mellor, Andrew, Woodgate, William, Soto-Berelov, Mariela, Haywood, Andrew, Skidmore, Andrew K., 2015. Mapping Forest canopy height across large areas by upscaling ALS estimates with freely available satellite data. Remote Sens. 7 (9), 12563–12587.
Wulder, Michael A., Bater, Christopher W., Coops, Nicholas C., Hilker, Thomas, White, Joanne C., 2008. The role of LiDAR in sustainable Forest management. The Forest. Chron. 84 (6), 807–826.

Wulder, Michael A., White, Joanne C., Nelson, Ross F., Næsset, Erik, Ørka, Hans Ole, Coops, Nicholas C., Hilker, Thomas, Bater, Christopher W., Gobakken, Terje, 2012. Lidar sampling for large-area Forest characterization: a review. Remote Sens. Environ. 121, 196–209.

Yip, Ka Hei, Anson, Rui Liu, Jin, Wu, Hau, Billy Chi Hang, Lin, Yinyi, Zhang, Hongsheng, 2024. Community-based plant diversity monitoring of a dense-canopy and species-rich tropical Forest using airborne LiDAR data. Ecol. Indic. 158, 111346.

Zellweger, Florian, Braunisch, Veronika, Baltensweiler, Andri, Bollmann, Kurt, 2013. Remotely sensed Forest structural complexity predicts multi species occurrence at the landscape scale. For. Ecol. Manag. 307, 303–312.

Zellweger, Florian, De Frenne, Pieter, Lenoir, Jonathan, Vangansbeke, Pieter, Verheyen, Kris, Bernhardt-Römermann, Markus, Baeten, Lander, Hédl, Radim, Berki, Imre, Brunet, Jörg, 2020. Forest microclimate dynamics drive plant responses to warming. Science 368 (6492), 772–775.

Zhang, Zhengnan, Cao, Lin, She, Guanghui, 2017. Estimating Forest structural parameters using canopy metrics derived from airborne LiDAR data in subtropical forests. Remote Sens. 9 (9), 940.

Zhang, Zhenyu, Liu, Xiaoye, Peterson, Jim, Wright, Wendy, 2011. Cool temperate rainforest and adjacent forests classification using airborne LiDAR data. Area 43 (4), 438–448.

Zhao, Feng, Strahler, Alan H., Schaaf, Crystal L., Yao, Tian, Yang, Xiaoyuan, Wang, Zhuosen, Schull, Mitchell A., Román, Miguel O., Woodcock, Curtis E., Olofsson, Pontus, 2012. Measuring gap fraction, element clumping index and LAI in sierra Forest stands using a full-waveform ground-based Lidar. Remote Sens. Environ. 125, 73–79.

Zhao, Kaiguang, Popescu, Sorin, Nelson, Ross, 2009. Lidar remote sensing of Forest biomass: a scale-invariant estimation approach using airborne lasers. Remote Sens. Environ. 113 (1), 182–196.

Zhao, Kaiguang, Popescu, Sorin, Meng, Xuelian, Pang, Yong, Agca, Muge, 2011. Characterizing Forest canopy structure with Lidar composite metrics and machine learning. Remote Sens. Environ. 115 (8), 1978–1996.

Zimble, Daniel A., Evans, David L., Carlson, George C., Parker, Robert C., Grado, Stephen C., Gerard, Patrick D., 2003. Characterizing vertical Forest structure using small-footprint airborne LiDAR. Remote Sens. Environ. 87 (2–3), 171–182.